Journal Pre-proof

Implications of transient methane flux on associated biological communities in high-arctic seep habitats, Storbanken, Norwegian Barents sea

Taylor P. Heyl, Giuliana Panieri, Daniel J. Fornari, Rune Mattingsdal, Simone Sauer, Haoyi Yao, Luke McCartin, Elisabeth McElwee, Timothy M. Shank

PII: S0967-0637(23)00195-4

DOI: https://doi.org/10.1016/j.dsr.2023.104156

Reference: DSRI 104156

To appear in: *Deep-Sea Research Part I*

Received Date: 29 March 2022

Revised Date: 4 September 2023

Accepted Date: 11 September 2023

Please cite this article as: Heyl, T.P., Panieri, G., Fornari, D.J., Mattingsdal, R., Sauer, S., Yao, H., McCartin, L., McElwee, E., Shank, T.M., Implications of transient methane flux on associated biological communities in high-arctic seep habitats, Storbanken, Norwegian Barents sea, *Deep-Sea Research Part I* (2023), doi: https://doi.org/10.1016/j.dsr.2023.104156.

Implications of Transient Methane Flux on Associated Biological Communities in High-Arctic Seep Habitats, Storbanken, Norwegian Barents Sea

Taylor P. Heyl[a,*], Giuliana Panieri[b], Daniel J. Fornari[c], Rune Mattingsdal[d], Simone Sauer[e], Haoyi Yao[b], Luke McCartin[a,f], Elisabeth McElwee[a], and Timothy M. Shank[a]

[a] Biology Department, Woods Hole Oceanographic Institution, 266 Woods Hole Rd., Woods Hole MA 02543, USA

[b] Centre for Arctic Gas Hydrate, Environment and Climate, CAGE, Department of Geosciences, UiT – The Arctic University of Norway, N-9037, Tromsø, NO

[c] Geology and Geophysics Department, Woods Hole Oceanographic Institution, 266 Woods Hole Rd., Woods Hole MA 02453, USA

[d] Norwegian Petroleum Directorate, N-9407 Harstad, NO

[e] IFREMER, France IFREMER-Institut Francais de Recherché pour l'Exploitation de la Mer, Plouzane, FR

[f] Department of Biological Sciences, Lehigh University, 27 Memorial Drive West, Bethlehem, PA 18015, USA

Keywords: climate change, crater, folliculinid ciliates, methane flares, methane seep, microbial mats

*__Corresponding Author__:

Taylor P. Heyl

Biology Department, MS33 Redfield Laboratory

Woods Hole Oceanographic Institution

266 Woods Hole Rd, Woods Hole MA 02543

theyl@whoi.edu

Tel. (508) 289-2279

Highlights

- Abundant methane flares observed along the Norwegian margin prior to 2015 and reduced number of flares detected in 2017, together with low methane concentrations measured in the sediment, suggest an inter-annual transient seep environment
- Metazoan community structure within the Storbanken Crater area in the Barents Sea revealed high diversity and differences between crater and non-crater sites
- We present the first evidence of methane release and flux with microbial mat distribution and associated folliculinid ciliates
- No chemosynthetic megafaunal species were observed among areas of seep expression in the areas surveyed
- We provide baseline information on the temporal release of arctic methane and benthic biological communities, initiating temporal studies to identify future changes and predict the impacts of climate change

Abstract

The continental margins of the Arctic Ocean basin contain methane seeps, where transient fluxes of seafloor methane are released due to the thermal dissociation of gas hydrates. An increase in shallow methane seeps identified over the past decade, potentially due to enhanced warming of the Arctic Ocean bottom water and associated destabilization of hydrate structure. Biological communities associated with methane release east of Svalbard in the Barents Sea (Storbanken Crater site, 76° 46.7'N, 35° 43.5'E, depths between 120 m – 300 m depths) were investigated using towed camera imagery and ship-based platforms during a 2017 CAGE17-2 cruise on the RV *Helmer Hanssen*. We analyzed relationships among methane flux data, seafloor habitat characteristics, and biological community structure (i.e., presence and distribution of megafauna and expression of microbial mats) from a total of 14 surveys (6,827 images and 40 multicore sediment cores) within the Storbanken Crater area and compared it to 2015 data. Unlike seep expressions at deeper sites (~ 1200 m) in the Norwegian margin region, no seep-endemic, chemosynthetic-associated megafaunal species were observed at the shallow surveyed sites and all sites hosted similarly diverse communities of non-seep species, including commercially important fish and crustaceans. Methane concentrations did not markedly differ between the crater and non-crater sites. Rates of methane gas advection through sediments (in the form of flares) were relatively low and concentration of methane was even lower in porewater samples at the crater site. We present the first evidence of methane flare flux and intermittent microbial mat distribution with associated folliculinid ciliates, which suggests a long history of methane emissions and a transient seep environment in spatial and temporal flux. Together, this study presents a critical baseline on the temporal release of arctic methane and benthic biological communities to initiate temporal studies that identify future changes and predict the impact of climate change.

1. Introduction

Cold seeps occur along continental margins worldwide, where hydrocarbons such as methane and other reduced chemicals are emitted through soft sediments commonly associated with pockmarks, craters, carbonate mounds, gas hydrates or underwater pingos (Dando et al., 1991; Lammers et al., 1995; Hovland and Svensen 2006; Ritt et al., 2011; Zeppilli et al., 2012, Suess, E., 2014). Methane seeps have worldwide distribution and are known to exist along the margins of the Arctic Ocean that have the potential to be affected by dynamic changes in temperature, tectonic processes, and ocean circulation (Spielhagen et al., 2011). Seafloor methane release in the Arctic (e.g., Sahling et al., 2014; Shakhova et al., 2014; Smith et al., 2014; Westbrook et al., 2009) is of particular interest as evidence suggests ocean warming is amplified in polar regions (e.g., Parmentier and Christensen, 2013) where many sources and reservoirs of methane, in the form of frozen hydrates are climate sensitive (e.g., Ruppel and Kessler, 2017, Fisher et al., 2011).

The sources of hydrocarbon release from seeps in the Arctic is poorly understood, yet are critical for untangling the feedback loop between cold seeps ecosystems and climate change. An escape of methane, a potent greenhouse gas (Lashof & Ahuja, 1990, MacDonald 1990), from the Arctic seafloor could have profound implications on Arctic biogeochemical cycles, biological community diversity, oceanographic and global climate change, particularly if methane gas is able to reach the atmosphere (Dickens et al., 1997; Kennett et al., 2000; 2003; Borges et al., 2016). The release of methane from shallow (< 500 m) seafloor depths could contribute to increased temperatures in the Arctic (Ruppel, 2011). Notably, evidence exists that warming of hydrate-bearing sediments between 17,000 and 15,000 years ago led to large-scale methane emissions (Andreassen et al., 2017; Serov et al., 2017; Dessandier et al., 2021). Arctic continental shelves host vast amounts of methane in the form of hydrates; frozen mixtures of gas and water trapped in a crystalline lattice. The stability of methane hydrates is dependent on low temperatures and high pressures in the Arctic sedimentary layers (Ruppel and Kessler, 2017). As the Arctic waters warm (e.g., Spielhagen et al., 2011; Lind et al., 2018), the potential grows for increased release of methane out of the hydrates and into the water column (O'Connor, 2010; Ferre´ et al., 2012; Thatcher et al., 2013; Ferre´ et al., 2020).

Following the first visual inspection of active release of hydrocarbons from a pockmark in the North Sea in 1985 (Hovland and Sommerville, 1985, Hovland and Judd, 1988), large regions of seafloor hydrocarbon seepage off the nearby continental shelves were discovered associated with seabed craters in the northern Norwegian continental shelf in the western Barents Sea (Elverhoi and Solheim, 1989, Åström et al., 2020). These seeps are thought to be associated with deep-seated fault systems, and the result of fluid migration through the sedimentary layers due to glacial unloading and erosion (Chand et al., 2012). West of Prins Karls

Forland in the inter-fan region between the Isfjorden and Kongsfjorden cross-shelf troughs, the majority of methane seeps occur between 360 and 415 m water depth (Figure 1) (Sahling et al., 2014; Westbrook et al., 2009; Ferre´ et al., 2021). Seismic surveys indicate the presence of shallow gas in the upper continental margin sediments, and shallow methane hydrate deposits further offshore (Chabert et al., 2011; Rajan et al., 2012; Sarkar et al., 2012). Gas migration appears to occur through permeable hemipelagic sediment sequences, which are variably capped by less permeable glacigenic sediments on the upper slope and shelf (Rajan et al., 2012; Sarkar et al., 2012; Thatcher et al., 2013).

Recent investigation of sampled faunal and infaunal communities near and in cold seeps in the Barents Sea ecosystem have indicated that: (1) strong, localized effects (over small spatial scales) of seeps, support dense communities of small endosymbiotic frenulate siboglinid polychaetes that play a fundamental role in structuring the seabed animal community (Sen et al., 2018); (2) these cold seeps provide heterogeneous substrates and food resources independent of photosynthetic sources from the surface ocean (revealing a co-located mixture of chemosynthetic and non-chemosynthetic taxa) (Decker & Olu, 2012); (3) methane-derived carbon is incorporated into the food web of the non-seep Barents Sea ecosystems (Åström et al., 2019); and that (4) further investigation of these faunal-habitat associations are necessary to understand how ecosystems may respond to temporal and hydrocarbon changes in seep environments (Sen et al., 2018).

The Barents Sea is an economically important region supporting one of the richest fisheries in the world and the Storbanken Crater site on the Northern Arctic flank is located in a commercially significant and ecologically sensitive area that has been recently impacted due to fishing activity, particularly trawling, which actively affects the sedimentary layers of the seafloor, disrupting associated benthic habitats. The discovery of methane flares and potential for their transient and highly mobile nature now places a premium on understanding the rates of temporal changes and the associated response in faunal community structure (Kannberg et al., 2013; Gentz et al., 2014). Based on this discovery, we expected that the seep expressions and methane fluxes within the Storbanken Crater system would be transient with some sites experiencing flare extinction and new seep expression. Such a finding would be consistent with modern studies of the rates of habitat turnover and growth, species recruitment, and ecosystem recovery in other seep systems (Lessard-Pilon et al. 2010, Pereira et al. 2021).

The Arctic, and particularly the Barents Sea, are predicted to experience intensified impacts of climate warming within the next two decades, such as shrinking sea ice cover, changing oceanographic patterns and increasing acidification (Haug et al., 2017; Onarheim and Arthun, 2017; Weslawski et al., 2011). To address questions of temporal dynamics of regional seepage and establish a baseline of observations from which to document future changes in seep flux and biological community structure in the Arctic, we characterized the: (1) distribution of geological and biological characteristics from multibeam and *TowCam* towed-camera imagery during the 2017 CAGE 17-2 cruise; (2) the distribution of methane and composition of gas flares during the MAREANO 2015 survey and analysis of sediment pore water methane in 2017 (3) faunal-habitat associations from each of the 2017 *TowCam* tows. From these data, we observed a wide distribution of microbial mats and authigenic carbonates associated with folliculinid ciliates, suggesting an inter-annual transient seep environment in flux in the Storbanken Crater area. This site is of particular interest given its shallow water location may allow the release of gaseous methane through soft sediment into the water column, ultimately emerging into the atmosphere at high flux (Rehder et al., 1998; Platt et al., 2018).

2. Methods

2.1. Geological Setting

The Storbanken Crater area is located east of Svalbard in the Barents Sea (76° 46.7’N, 35° 43.5’E), in water depths of 120 m to 300 m (Figure 1). The bathymetrical high of Storbanken is a seafloor representation of a large geological high in the sub-surface, and the crater site is located on the southern part of this high on a large eroded and faulted structural closure that acts as a focal point for hydrocarbons migrating upwards from deeper source rocks (2A). The source rock of migrating hydrocarbons in the area is unconfirmed, but most likely of Early to Middle Triassic age (~251 to 237 Ma) (Lundschien et al., 2014, Weniger et al., 2019). This site is characterized by the presence of large (up to 900 m in diameter and 10 to 30 m deep) depressions that are interpreted to have formed either catastrophically (Andreassen et al., 2017) or more gradually due to methane hydrate dissociation during isostatic rebound following deglaciation (Andreassen et al., 2017; Nixon et al., 2019).

2.2 Seismic Data and Methane Flare Mapping

Seismic data were acquired from two regional surveys conducted by the Norwegian Petroleum Directorate (NPD) in 2012 and 2013, which consisted of a regular 3 to 4 km x 13 km grid of industry multi-channel 2D seismic data within the study area. The interpretations are part of NPD’s regional studies in the area, and all seismic horizons had age control from shallow boreholes and regional seismic correlations (R. Mattingsdal, pers. comm.). Gas flares were mapped from multi- and singlebeam echosounder water column data in FMMidwater (© Quality Positioning Services B.V. 2020) and exported as ASCII XYZ data for filtering based on amplitude using a MATLAB™ script. Gas flares over the central crater depressions were mapped prior to the 2017 CAGE17-2 cruise using data from MAREANO, a program coordinated by the Institute of Marine Research that maps depth and topography, sediment composition, biodiversity, habitats and biotopes, and pollution in the seabed in Norwegian coastal and offshore regions. The bathymetry of the area was mapped by MAREANO in 2015. Additional multibeam surveys were performed during the 2017 CAGE17-2 cruise, primarily focused on identifying gas flares.

Acoustic anomalies identified as gas flares typically had a stronger response on the lower frequency (18kHz and 38kHz) singlebeam echosounder (EK60) channels. By contrast, acoustic anomalies that appear to be associated with fish/krill had a strong response at 120kHz but were much weaker at the lower frequencies (see Figure 2). This contrast in frequency response was used to distinguish gas flares from schools of fish during the acoustic surveying of the Storbanken Crater site. Gas flare locations from both 2015 and 2017 were used to target the collection of sediment samples and to position *TowCam* survey tows. Based on these flare locations, we hypothesized that methane was emitted from the craters and that these craters could potentially host biological communities associated with seeps.

2.3 Seafloor Imagery

We collected seafloor imagery using the towed imaging system, *TowCam* (Figure 3), which was operated through the WHOI-MISO (Multidisciplinary Instrumentation in Support of Oceanography) Facility on the RV *Helmer Hanssen*, cruise number CAGE17-2, from June 21 to July 03, 2017. *TowCam* is an internally recording, 6000 m rated, digital, down-looking deep-sea imaging system that also acquires camera altitude and CTD water properties data. Images were acquired every 10 seconds using the MISO Ocean Imaging Systems Nikon D3300 24-megapixel camera with a Nikkor 20 mm lens, at an altitude between 2 to 4 meters from the seafloor at a speed of ~ 0.25 kts. *TowCam* was equipped with two vertical lasers separated by 20 cm for scale and co-registered to a CTD sensor (SeaBird SBE25) and an altimeter to provide accurate depth and altitude for each image. The images from the *TowCam* system were recorded internally and simultaneously transmitted to the surface through a 0.68” CTD cable for real-time observation. The *TowCam* was towed from a standard 0.322" 3-conductor CTD sea cable, that permitted real-time acquisition of digital depth and altitude data used to aid in the analysis of digital images, and in creating accurate near-bottom topographic profiles. A forward-looking altimeter was used for obstacle avoidance during the tows. Images were geo-referenced from the ship’s GPS and an acoustic USBL beacon on *TowCam* to identify and document seafloor features, including seep and non-seep areas within each site.

The KC Denmark DK8000 6-core multicore system was modified into a real-time imaging platform for *TowCam* to assess sites prior to sampling and then deployed (Figure 3B) to obtain 6 simultaneous push cores (deployed 4 times per site) for methane and pore water analyses. We completed a total of 14 lowerings at the Storbanken Crater site between June 21 to July 03, 2017, which produced a total of 6,827 seafloor images and 40 multicore sediment samples (Table 1).

2.4 Methane Geochemistry

Pore water samples were taken from one of the six multicores at each multicore lowering by the KC Denmark DK8000 6-core multicore system (Table 2). 20 ml acid-washed syringes were attached to the rhizons for pore water collection. Rhizons were inserted through pre-drilled holes in the liner at intervals ranging between 2 and 10 cm. Depending on the amount of pore water collected, the samples were split for onboard analysis of alkalinity and dissolved Fe^{2+} concentration, and onshore analysis of dissolved inorganic carbon (DIC), δ^{13}C-DIC (addition of $HgCl_2$) and cations (acidified with nitric acid). Headspace methane samples were taken from the same multicore as the pore water. Methane samples were collected using cut-off syringes to retrieve 3 ml of sediment, which was transferred to serum vials containing two glass beads and 6 ml 2.5% NaOH solution. Before closing the vials they were flushed with N_2, and afterwards stored at 4°C until analysis.

For onboard analysis of alkalinity and dissolved Fe^{2+}, alkalinity was first titrated with pH control. The pH electrode was calibrated prior to the cruise. 0.012M HCl was prepared before the cruise and calibrated daily against a 0.01 M Borax standard solution and local seawater. An aliquot of 1 mL of pore water was used for alkalinity titration, 5-10 mL of 0.7 M KCl was added to ensure the pH electrode was fully submerged. Acid was added slowly with stir bar stirring. The amount of acid and pH was manually recorded for at least five points to calculate the alkalinity from the Gran function plots.

The concentration of dissolved Fe^{2+} in pore water samples was determined using a spectrophotometer (Shimadzu UVmini 1240 UV) measuring the adsorption at a wavelength of 560 nm after the formation of a color complex with a commercial ferrospectral solution (Collins et al. 1959). The calibration was based on the measurement of solutions with known $Fe2^{+}$ concentration ranging between 0.05 and 0.5 ppm. If the Fe^{2+} concentration of the samples was higher than 0.5 ppm, the sample was diluted with O_2-free MilliQ water.

Onboard analysis of methane concentration was performed with a ThermoScientific Trace 1310 gas chromatograph equipped with a ThermoScientific TG-Bond Alumina (30 m x 0.53 mm x 10 µm) column and a flame-ionization detector (GC-FID). Methane concentration in the pore water was calculated assuming a constant porosity of 0.8. Additionally, cation concentration of the pore water samples was determined by inductively coupled plasma atomic emission spectrometry (ICP-AES) at the Geological Survey of Norway laboratory using a Perkin Elmer Optima 4300 Dual View. Samples were diluted 1:40 before analysis.

δ^{13}C-DIC was determined on a Gas-bench couple to MAT 253 at Stable isotope lab SIL at the Department of Geosciences at UiT. Sediment porewater was extracted through rhizon filters to 5 mL syringes. Microbial activity was quenched by the addition of saturated $HgCl_2$. The analysis of δ^{13}C of DIC was conducted by adding 0.5 mL of sample to 4.5 mL vials, preflushed with He and 4-5 drops of H_3PO_4 added. The samples were in equilibration for more than 24 hours at 24 degrees C and then calibrated by simultaneous analysis of 3 solid calcite standards with δ^{13}C values that enclose the values of the samples. We corrected the measured δ^{13}C values by -0.1 per mil, to account for fractionation between gas and aqueous in the samples.

An aliquot of pore water was placed in specific vials and flushed with He gas prior to addition of 5 drops of anhydrous phosphoric acid and equilibrated at 50°C for over 3 hours. The liberated gas was then analyzed on the Isotope ratio mass spectrometer. The δ^{13}C values are reported in per mil ‰ relative to the Vienna Pee Dee Belemnite (VPDB) standard. The analytical precision of δ^{13}C was greater than 0.07 ‰ by measuring the certified standard NBS-19.

2.5 Biological Community and Habitat Structure

Each *TowCam* seafloor image was visually screened and scored independently by the authors (LM, EM and TPH) for habitat type and all observable fauna. Observable megafauna were identified and sorted into different taxonomic groups based on morphological similarity, and the presence/absence of each taxon was scored for each image using iView MediaPro (ver. 3.1.3 iView Multimedia Ltd). Animals were identified using publicly available reference images (NOAA Ocean Exploration Benthic Deepwater Animal Identification Guide) and published taxonomic keys. The presence of microbial mats in each image was also recorded. There were no analyses of infauna from the 40 multicore samples taken but the smallest size of organisms visible in the images analyzed was approximately 1 to 2 cm, based on 20 cm scaling lasers parallel to the *TowCam* camera axis.

The habitat type in each image was classified as: sediment, drop stones, outcrops, trawl marks and microbial mats). These data from each *TowCam* lowering were exported from the iView MediaPro catalog and merged with *TowCam* USBL navigation, depth, and CTD data using the time-date stamp from the image file names.

Geo-referenced habitat, environmental data (e.g., methane), and megafaunal presence, were inputted into ArcGIS (Version 10.6.1) and layered on high-resolution bathymetry maps to yield faunal habitat association maps. Data from ArcGIS were used to address the spatial and temporal fractions of the questions above.

3. Results

3.1 Sub-surface geology and seafloor characterization

Through geo-referenced shipboard mapping of sub-surface geology seafloor and methane flares, we observed that gas leakage from the seafloor occurred primarily along faults offsetting the seafloor in this region, at the crest of reservoir sandstones with eroded cap rocks, and/or where reservoir sandstones were sub-cropped at the seafloor (Figure 2B). Acoustic anomalies identified as gas flares typically had a stronger response on the lower frequency (18kHz and 38kHz) singlebeam echosounder (EK60) channels. Ship-based mapping of acoustic flares at this site in 2015 and 2017 noted dramatic differences in the locations and abundance of methane bubble plumes (Figure 4). All of the flares observed during the CAGE 17-2 survey correspond to acoustic water column anomalies identified in the MAREANO 2015 dataset. The smaller acoustic anomalies from the MAREANO 2015 dataset were not observed during the CAGE 17-2 survey.

The *Towcam* tows were clustered within the Storbanken Crater (5 *TowCam* surveys) and within non-crater areas (9 *TowCam* surveys, Figure 5). The seafloor habitat classification of the *Towcam* images revealed five distinct seafloor characteristics; drop stones, outcrops, and sediment, microbial mat and trawl marks (Figure 6A). The seafloor inside and outside the craters was dominated by vast expanses of soft (muddy) substrate interspersed with larger scale characteristics such as depressions, rock slabs, carbonate crusts, drop stones and rocky outcrops (Figure 7). Microbial mats were observed throughout the non-crater site (Figure 7). We observed distinct trawl marks creating depressions through the soft sediment in more than 18 images at the non-crater Storbanken site (*TowCam* # HH942-23) (Figure 6C). No trawl marks were observed within the crater site.

3.2 Methane Geochemistry

The pore water composition and the methane concentration of seven multicores and three gravity cores was analyzed over the area where acoustic gas flares were observed (Figure 4). The methane concentration in all cores was relatively low (< 10 µmol/l). The highest concentration of methane detected was 6 µmol/l in the multicores (MC-939) and 3.5 µmol/l in the gravity cores (GC-935) (Figure 1, supplementary material). Dissolved Fe^{2+} was detected in almost all samples, with highest concentrations up to 289 µmol/l in the upper centimeters of MC-933 (Figure 3). Fe^{2+} concentrations only dropped below 4 µmol/l towards the base of MC-939 and MC-957. In all the other cores and across all core sample depths, Fe^{2+} remained relatively high throughout the core. Ca^{2+} concentrations remained constant throughout all cores with an average ~ 9.2 mmol/l. Sr^{2+} and boron concentrations remained constant throughout all the multicores with averages of 82 µmol/l and

368 μmol/l, respectively (Figure 2, supplementary material). In the two gravity cores GC-971 and GC-972, there was an increase in Sr^{2+} observed at the base of the cores with values up to 118 μmol/l (Table 1, supplementary material). In the same gravity cores, a decrease in boron concentration could be observed from the base of the cores down to 277 μmol/l.

Alkalinity, dissolved inorganic carbon (DIC), and δ^{13}C-DIC were measured on selected multicores (Figure 3, supplementary material). Alkalinity and DIC increased only slightly with depth in the multicores. The greatest increase was detected in MC-939 with an alkalinity up to 4.7 mmol/l and DIC up to 2.9 (mmol/l).

3.3 Biological Community and Habitat Structure

The composition and distribution of species varied among sites and habitats varied within each site (8A and 8B; Table 3). Microbial mats (and authigenic carbonate crust indicative of previous emissions of methane through the seafloor) were present between 150 to 160 m at the OBC-M1 and D3 sites, in markedly greater abundance at the D3 site, and not observed at other sites (between160 to 220 m depth). Mats were absent from the crater site but they were observed at the non-crater site (Figure 6). Patches of thin microbial mats (typically forming layers ~1to 2 mm thick and ca 20 cm in diameter) were observed on soft sediments, displaying irregular surface morphologies and complex networks (Figure 6B). These microbial mats were widely distributed throughout the non-crater site.

Known chemosynthetic fauna were not observed at either the crater or the non-crater site and the absence of large symbiont-bearing chemosynthetic taxa (i.e., mussels, clams, tubeworms) was noted. The microbial mats at the seep sites in this study exhibited distinct characteristics of folliculinid ciliates known to be associated with seeps in a variety of substrates, including authigenic carbonates (Pasulka et al., 2017). Though we were not able to visually identify to genus level, many species are recognizable by a distinct blue coloring, similar to those observed at the Storbanken sites (see Figure 6B).

Both areas hosted diverse non-chemosynthetic invertebrate communities that were presumed to be utilizing hard substrate provided by the methane-derived authigenic carbonates as a platform for establishment (Levin et al., 2015). A broader diversity of echinoderms (crinoids, sea cucumbers, sea stars and ophiuroids) was present at the non-crater site (Figure 8). Crinoids, passive suspension feeders attracted to moving ocean currents and therefore used as indicators of bottom current direction, were observed only at the non-crater site. Interestingly, crinoids densely populated the top of the shallow mound (*TowCam* # HH942-TC17, 160 m) at the crater site (where no methane flares were observed, see Figure 2b), which was distinct from the other crater site areas.

Cnidarians (e.g., nephtheid soft corals and anemones) were observed in sediment, particularly at the crater site, but along with sponges, holothurians (cf. *Psolus*), and ophiuroids, they were present at all sites (Table 3). Epifaunal colonization of drop stones and outcrops on the surface seafloor was a common observation (e.g., anemones, sponges, etc.) and various diverse and commercially important fish communities inhabited both sites, although flatfish (likely *Hippoglossoides platessoides* of two age classes) and schooling fish were observed more frequently at the crater site (Table 3). Arthropods, including abundant pycnogonid sea spiders (present at OBC-NE, D1, and C1), less abundant pagurid crabs (present only at D3 and D4) and brachyuran crabs (only at D1 and C1) as well as molluscs, in the form of gastropods (only at D3 and D4) and an octopus (only at D1) were present in the sediment at these sites (Table 3).

4. Discussion

4.1 Methane and the importance of climate change in the Arctic

Methane is a significant greenhouse gas and understanding methane release in the Arctic is critical to assessing its future impact on global climate change. It is well known that the most common sources of methane in the marine environment originate either from the thermocatalytic breakdown of complex organic matter at temperatures above 150°C (producing thermogenic methane) or microbial methanogenesis, producing microbial methane (Judd, 2004), at temperatures below 80°C. An increase in seawater temperatures in the Arctic can lead to an increase in methane emissions, which then contribute to positive feedback loops further accelerating Arctic warming and global climate change. During previous expeditions at the Storbanken sites, flare signals and microbial mats on the seafloor were observed at the non-crater site, but were absent at the crater site, with the exception of the small mounds in the crater where methane releases in the water column were present. This suggests that these small mounds, areas of higher topographical relief, are associated with deep gas migration channels, as suggested by similar features in the leakage system at Storfjordrenna (Serov 2017; Waage et al., 2020).

There was no visual observation of oil or other petroleum release. Sediment was concentrated in depressions and could extend to 50 meters depth, however multicore and gravity cores sampled up to 2 meters of sediment exhibited very low methane concentrations. The low methane concentrations in the water column (the highest concentration observed in multicores was only 6 µmol/l and even less in the deeper gravity cores, see Table 1 supplemental material, and background/non-seep environments had no methane in the sediment) compared to concentrations at other Arctic seep sites (Sen, 2018), further indicated that there was weak or inactive methane seepage in the depressions. The number of methane flares observed in 2015 was reduced by more than 50%

when investigated in 2017. The high abundance of flares in previous MAREANO surveys, and the reduced number detected in 2017, together with the measured low sediment methane concentrations, suggest that the methane flow within this system is either decreasing or presently transitioning from active to inactive.

Although some multicores were sampled proximal (10s of meters) to microbial mats, the mats were not captured in the core samples and we observed no evidence of methane seepage in any of the cores. If we assume that the acoustic gas flares represent methane escape from the seafloor, this could mean that the gas ascent is highly localized and that methane concentrations present high gradients over the sediment surface, on the order of 10s of centimeters away from a fluid pathway. There is also the possibility that higher methane concentrations exist in this system but that methane is trapped in the form of gas bubbles or hydrates in the sediments and therefore not emitted into the water column, and thus do not produce an acoustic signal (Luo et al., 2016, Bravo et al. 2021, 2022).

Moreover, the analyzed pore water showed no indications of anaerobic oxidation of methane. Clear signs of anaerobic oxidation of methane would indicate an increase in alkalinity (up to 30 mmol/l), due to HCO^{3-} and HS^{-} production, a decrease in Ca^{2+} concentration due to authigenic carbonate formation, and strong decreases (below -40 ‰) in δ^{13}C-DIC (e.g., Boetius et al., 2000; Ussler and Paul 2008, Hong et al., 2016). None of these indicators were detected in our multicores and gravity cores. However, a notable increase in Sr^{2+} and a decrease in boron concentration towards the base of GC-971 and GC-972 were detected. These gravity cores were retrieved from depression D1 (*TowCam* # HH942-14, Figure 5a). This could suggest the ascent of a fluid rich in strontium and poor in boron, but low in methane concentration at this site. It could also indicate a diagenetic process that releases strontium and consumes boron.

4.2 Linkages between methane flares, distribution of microbial mats and biological communities

The transient nature of the seepage observed during the different years of surveying (2015 and 2017) can likely be explained by a combination of differences in the: (1) tidal cycles during surveys; (2) presence of stable gas hydrates clogging the hydrocarbon migration pathways; (3) regional pressure in the sub-surface reservoirs where the gas is escaping (initiated by seismic events or episodic release of gas related to build-up of pressure as gas migrated into the reservoir from an active source rock below); (4) differences in biological, oceanographic and/or technical noise in the water column making data interpretations of gas flares uncertain; and/or (5) processes conveying waning in a transient methane system. It is well known that methane seepage can vary on tidal, lunar and inter-annual time scales (e.g., Lee and Huatala 2021, Di et al. 2014, Tryon et al. 2002). While tidal measurements were not taken during this study, we recognize the importance of tidal information in order to assess changes in methane concentrations and emissions from the seafloor (Römer et al., 2016, Boles et al., 2001, Torres et al., 2002). We also recognize that the smaller acoustic anomalies in the MAREANO 2015 dataset may have been produced by fish (schooling fish were abundantly observed during the CAGE 17-2 survey), which could have caused technical noise in the water column data, creating challenging interpretations of gas flares. Gas leakages in this area occurred primarily along faults, which provided a pathway for the release of gases and fluids from the seafloor in the form of flaring, indicative of methane emissions. These leakages could have ceased through smaller flow pathways between 2015 and 2017. Gas hydrates blocking methane migration pathways and regional pressure differences are both possible explanations for the observed changes in methane but because methane flares and concentration of methane were both reported higher in 2015, we suspect a waning or presently transient methane system is more likely to account for the reduction in methane release.

Although we observed that the faunal communities were similar among the Storbanken Crater sites, the sites fundamentally differed in the expression of hydrocarbon seepage. The methane concentration overall in these sites was lower than observed in other areas of the Barents Sea (Sen, 2018), suggesting that the expression of seepage within the system appears to be transient and affecting community structure (micro/macro biology integration). Microbial mats were observed where carbonates were also observed, indicating a long period (on the order of decades) of fluid release, which may suggest either temporal periods of change from methane flux to no methane flux or a temporal on and off that can be related to methane flare observations. Seep expressions in the form of microbial mats exist in soft sediment environments with siboglinid frenulate tubeworms as observed at the Pingos sites (Sen et al., 2018) and also in environments without any evidence of chemosynthetic-based species as in the Storbanken Crater sites (this study). Based on the analyses of imagery, a lack of frenulates from the Storbanken sites has important ecological implications, as they are the only confirmed endemic chemosynthetic species in this Arctic region. Because all frenulates have obligate bacterial endosymbionts (Fisher, 1990; Hilario et al., 2011; Southward, 1982; Southward et al., 2005) and thiotrophy is the dominant nutritional method for symbionts of *O. haakonmosbiensis* (Losekann et al., 2008; Pimenov et al., 2000), it is suspected that the Storbanken Crater seep environments are not producing sulfide in sufficient concentrations to support frenulate tubeworm communities but may have enough for follinculinid ciliates associated with the hard authigenic carbonate substrate underneath loose sediments on the seafloor.

Fe is an important nutrient in the marine system because it indicates the presence or absence of H_2S in the sedimentary environment. In environments with hydrogen sulfide present, the precipitation of iron sulfides would occur, which removes Fe^{2+} from pore waters (e.g., März et al., 2008). Therefore, if high Fe^{2+} is measured in the cores, this indicates that there is low or no H_2S present. Low or no Fe^{2+} indicates a higher H_2S concentration, in the form of FeS (Hong et al., 2020). The fact that we detected dissolved Fe^{2+} in all our cores indicates low or no hydrogen sulfide in the pore water, further suggesting that this environment does not have sufficient chemical energy to host many chemosynthetic organisms, although larger chemosynthetic taxa are not typically observed at shallow seeps (Dando et al., 2010).

The presence of carbonate on the seafloor indicates that there is a long history of methane emission in this area. It has been shown from other sites in the Barents Sea, not far from Storbanken, that the deglaciation (ca 18ka) and isostatic adjustment caused changes in the gas hydrate stability zone, with consequent methane expulsion (Crémière et al., 2016; Serov et al., 2017). There are seep communities associated with four gas hydrate mounds (pingos) and seabed methane release in the Western Barents Sea (76°N, 400 m depth), which were investigated in 2015, 2016 and 2017 using the towed camera system, *TowCam* and in 2015 with another ROV system (Sen et al., 2018, Figure 1). Through geo-referenced mosaic mapping and seafloor sediment sampling, Sen et al. (2018) observed numerous seafloor seep expressions hosting heterogeneous soft sediment habitats that included microbial mats, methane-derived authigenic carbonate concretions, and frenulate siboglinid worms likely containing sulfide-oxidizing symbionts, suggesting that high levels of seafloor methane seepage linked to sub-surface gas reservoirs support an abundant and active sediment methanotrophic community that maintains high sulfide fluxes. These seeps located hundreds of kilometers from the Storbanken Crater site exhibited high methane concentrations (Sen et al., 2018) although concentrations of this magnitude were not observed in any of the sites within Storbanken.

From the image mapping, methane flare data (over several years) and geochemical analyses in this study, we propose that seep expressions and methane fluxes in the Arctic are highly transient, with some seeps experiencing episodic methane release, extinction and new seep expression. Methane was not concentrated specifically in the Storbanken crater site and we observed methane emissions from the area around the crater, indicating a continued slow methane release across the entire study area and not localized within the crater. It is commonly believed that warming Arctic environments affected by global climate change will release greater amounts of methane (James et al., 2016). In this study, we report a decline in methane flux in the sample sites in and around Storbanken Craters and recognize that repeated surveys (particularly utilizing autonomous underwater vehicle and sensing technologies), that include co-located seafloor, sub-seafloor, and water column sampling, as well as tidal measurements in future studies is required in order to quantify the affects and linkages of physical, chemical, and biological change with methane release in the Arctic.

4.3 Implications for fisheries and anthropogenic impacts in the Arctic

The Barents Sea (Figure 1) is considered an ecological hotspot for the circumpolar Arctic and an economically important region supporting one of the richest fisheries in the world (Carroll et al., 2018; Huag et al., 2017; Wassmann et al., 2011). Deep-sea corals and other benthic communities are sensitive to the impacts of fishing gear and based upon our knowledge of recruitment, growth rates and age structure, recovery rates are extremely slow (e.g., Waller et al., 2007; Roark et al., 2009). Observations of the impacts of a single trawl tow through coral habitat in the Gulf of Alaska where 1000 kg of coral were landed, showed *Primnoa* and other coral taxa were caught on 619 of 541,350 hooks fished at 150-900 m depths and that several years later 7 of 31 colonies remaining in the trawl path were missing 80-99% of their branches and boulders with corals attached were tipped and dragged (Krieger, 2002).

Fishing on the deep reefs off the coast of Norway has been well documented (e.g., Fossa et al., 2000) and in a comparison of un-trawled and trawled cold water coral habitats in Norway, there is photo documentation of large *Paragorgia arborea* broken apart in areas that have been trawled and *Lophelia pertusa* reefs that have been demolished (Murray, 2009: color plate 28). Cold-water coral habitats in the Barents Sea have been impacted due to persistent trawling activity (Roberts, 2009), but little is known about the effects of anthropogenic activity within the Storbanken Crater area, which is located in a commercially sensitive and ecologically significant area on the Northern Arctic flank that until 2010 was disputed between Norway and Russia, due to the high potential for oil and gas resources. The crater site was only recently documented (Nixon et al., 2019), and although it is not open for petroleum activity, new fisheries (e.g., snow crab) have begun in this area. Effects of trawling in this area were observed in more than 18 images on the seafloor of the non-crater Storbanken site (*TowCam* # HH942-23, Figure 6C) and there were also trawl tracks present at the Pingos site (approximately 520 kilometers away) where a series of commercially important species, for example, Atlantic cod (*Gadus morhua*), the northern shrimp (*Pandalus borealis*), haddock (*Melanogrammus aeglefinus*) and various flat fishes such as Greenland halibut (*Hippoglos-soides platessoides*) and snow crab (*Chionoecetes opilio*) were observed in association with microbial mats (Sen et al., 2018).

Conclusion

There is a critical need for better understanding of anthropogenic impacts on seafloor arctic/crater ecosystems in order to create a baseline for temporal climatic studies of methane seep variability in the Arctic. Along with the detailed sampling that has taken place, these observations based on imagery provide a baseline for future studies of the timescales of faunal community change (including trophic relationships and contribution from seeps) in conjunction with local-scale changes in chemistry. With our limited knowledge of the timescales over which seep flux varies, ecological responses, and predictions of how methane release may be altered, it is difficult if not impossible to predict how methane-based benthic and pelagic ecosystems will respond to a changing Arctic. Baseline information on the distribution, environmental conditions, and associated communities is required to initiate temporal studies to construct predictive models, identify future changes and predict the impacts of climate change.

Author Contributions

GP, DF and TMS conceived and designed this study. GP was Chief Scientist of the CAGE expeditions and DF conducted *TowCam* fieldwork. GP, RM, and SS provided methane flare and porewater data. TPH, LM and EM conducted the analysis of imagery. TPH wrote the manuscript. All authors contributed to a draft of the manuscript and approved the final version of the manuscript.

Funding

This study was supported through the Centre of Arctic Gas Hydrate, Environment and Climate [CAGE - Project number 223259] and the Norwegian Petroleum Directorate (NPD).

Declaration of competing Interest

The authors declare that they have no known competing financial interests or personal relationships that could have appeared to influence the work reported in this paper.

Acknowledgements

The authors would like to thank all the members of the scientific party and the Captain and crew of the RV *Helmer Hanssen* during the 2017 research expedition. We thank Gregory Kurras who helped with field operations for the *TowCam*/multicorer and in processing data from the cruise team. Thank you to Matteus Lindgren, for providing the methane concentration measurements during the CAGE 17-2 cruise and to Sydney Nick for generating maps of the study area. We are grateful to Johanna Weston for editing and to anonymous reviewers for comments that resulted in a substantially improved manuscript.

References

Andreassen, K., Hubbard, A., Winsborrow, M., et al., 2017. Massive blow-out craters formed by hydrate-controlled methane expulsion from the Arctic seafloor. Science, 356(6341), 948–953. https://doi.org/10.1126/science.aal4500.

Åström E.K.L., Carroll, M.L., Sen, A., et al., 2019. Chemosynthesis influences food web and community structure in high-Arctic benthos. Mar Ecol Prog Ser. 629:19-42. https://doi.org/10.3354/meps13101.

Åström, E. K. L., Sen, A., Carroll, M.L., et al., 2020. Cold Seeps in a Warming Arctic: Insights for Benthic Ecology. Front. Mar. Sci., 21 Sec. Global Change and the Future Ocean, https://doi.org/10.3389/fmars.2020.00244.

Boetius, A., Ravenschlag, K., Schubert, C. J., et al., 2000. A marine microbial consortium apparently mediating anaerobic oxidation of methane. Nature 407(6804): 623-626.

Boles, J. R., Clark, J. F., Leifer, I., et al., 2001. Temporal variation in natural methane seep rate due to tides, Coal Oil Point area, California. *Journal of Geophysical Research: Oceans*, *106*(C11), 27077-27086.

Borges, A.V., Champenois, W., Gypens, N., et al., 2016. Massive marine methane emissions from near-shore shallow coastal areas. Scientific Reports 1-8, https://doi.org/10.1038/srep27908.

Bravo, M. E., Levin, L. A., Fiori, S. M., et al., 2021. Can no-bubble methane seeps affect biological traits of benthic macroinvertebrates in coastal systems? Estuarine, Coastal and Shelf Science, 261, 107525, https://doi.org/10.1016/j.ecss.2021.107525.

Bravo, C., De Nobili, M., Gambi, A., et al., 2022. Kinetics of electron transfer reactions by humic substances: Implications for their biogeochemical roles and determination of their electron donating capacity. Chemosphere, 286, 131755. https://doi.org/10.1016/j.chemosphere.2021.131755.

Carroll, J., Vikebø, F., Howell, D., et al., 2018. Assessing impacts of simulated oil spills on the Northeast Arctic cod fishery. Marine Pollution Bulletin, 126, 63–73. https://doi.org/10.1016/j.marpolbul.2017.10.069.

Chabert, A., Minshull, T. A., Westbrook, G. K., et al., 2011. Characterization of a stratigraphically constrained gas hydrate system along the western continental margin of Svalbard from ocean bottom seismometer data. J. Geophys. Res. 116, B12102, https://doi.org/10.1029/2011JB008211.

Chand, S., Thorsnes, T., Rise, L., et al., 2012. Multiple episodes of fluid flow in the SW Barents Sea (Loppa High) evidenced by gas flares, pockmarks and gas hydrate accumulation. Earth and Planetary Science Letters, 331–332, 305–314. https://doi.org/10.1016/j.epsl.2012.03.021.

Cochrane, S. K. J., Denisenko, S. G., Renaud, P.E., et al., 2009. Benthic macrofauna and productivity regimes in the Barents Sea – Ecological implications in a changing Arctic, J. Sea Res., 61, 222-233, https://doi.org/10.1016/j.seares.2009/01/003.

Collins, P. F., Diehl, H., & Smith, G. F., 1959. 2, 4, 6-Tripyridyl-s-triazine as reagent for iron. Determination of iron in limestone, silicates, and refractories. *Analytical chemistry*, *31*(11), 1862-1867.

Crémière, A., Lepland, A., Chand, S. et al. 2016. Timescales of methane seepage on the Norwegian margin following collapse of the Scandinavian Ice Sheet. Nat Commun 7, 11509, https://doi.org/10.1038/ncomms11509.

Dando, P. R., Austen, M. C., Burke, R. A., et al., 1991. Ecology of a North Sea Pockmark with an Active Methane Seep. Marine Ecology Progress Series 70, no. 1:49-63. Accessed May 21, 2020. www.jstor.org/stable/24816798.

Dando, P. R. 2010. Biological communities at marine shallow-water vent and seep sites. In *The vent and seep biota* (pp. 333-378). Springer, Dordrecht.

Decker, C. & Olu, K., 2012. Habitat heterogeneity influences cold-seep macrofaunal communities within and among seeps along the Norwegian margin – Part 2: contribution of chemosynthesis and nutritional patterns. Marine Ecology 33: 231-245, https://doi.org/10.1111/j.1439-0485.2011.00486.x.

Dessandier, P. A., Knies, J., Plaza-Faverola, A., et al., 2021. Ice-sheet melt drove methane emissions in the Arctic during the last two interglacials. *Geology*, *49*(7), 799-803.

Di, P., Feng, D., & Chen, D., 2014. In-situ and on-line measurement of gas flux at a hydrocarbon seep from the northern South China Sea. Continental Shelf Research, 81, 80–87, https://doi.org/10.1016/j.csr.2014.04.001.

Dickens, G. R., Castillo, M. M., & Walker, M. M., 1997. A blast of gas in the latest Paleocene: Simulating first-order effects of massive dissociation of oceanic methane hydrate. Geology 25(3), 259-262, https://doi.org/10.1130/0091-7613(1997) 025<0259:ABOGIT>2.3.CO; 2.

Elverhøi, A., Pfirman, S. L., Solheim, A. et al., 1989. Glaciomarine sedimentation in epicontinental seas exemplified by the northern Barents Sea. *Marine Geology*, *85*(2-4), 225-250.

Ferré, B., Mienert, J., Feseker, T., 2012. Ocean Temerature variability for the past 60 years on the Norwegian-Svalbard margin influences gas hydrate stability on human time scales. J Geophys Res. 117(C10). https://doi.org/10.1029/2012JC008300.

Ferré B., Jansson P., Moser M., et al., 2020. Reduced methane seepage from Arctic sediments during cold bottom-water conditions. Nature Geoscience 13:144-8.

Fisher, C.R., 1990. Chemoautotrophic and methanotrophic symbioses in marine invertebrates, Rev. Aquat. Sci. 2:399-436.

Fisher, R. E., Sriskantharajah, S., Lowry, D., et al., 2011. Arctic methane sources: Isotopic evidence for atmospheric inputs. Geophys. Res. Lett. 38, L21803, https://doi.org/10.1029/2011GL049319.

Fosså J. H., Mortensen P. B., Furevik, D. M., 2000. Lopheliakorallrev langs norskekysten forekomst og tilstand. Fisken og Havet 2:1–94.

Gentz, T., Damm, E., Schneider von Deimling, J., et al., 2014. A water column study of methane around gas flares located at the West Spitsbergen continental margin. Continental Shelf Research, 72, 107–118. https://doi.org/10.1016/j.csr.2013.07.013.

Haug, T., Bogstad, B., Chierici, M., et al., 2017. Future harvest of living resources in the Arctic Ocean north of the Nordic and Barents Seas: A review of possibilities and constraints. Fish. Res., 188 (Supplement C), 38-57, https://doi.org/10.1016/j.fishres.2016.12.002.

Hilário, A., Capa, M., Dahlgren, T. G., et al., 2011. New perspectives on the ecology and evolution of siboglinid tubeworms. PloS One 6(2), e16309. https://doi.org/10.1371/journal.pone.0016309.

Hong, W. L., Sauer, S., Panieri, G., et al., 2016. Removal of methane through hydrological, microbial, and geochemical processes in the shallow sediments of pockmarks along eastern Vestnesa Ridge (Svalbard). Limnology and Oceanography.

Hong, W. L., Latour, P., Sauer, S., et al., 2020. Iron cycling in Arctic methane seeps. Geo-Marine Letters, 40(3), 391–401. https://doi.org/10.1007/s00367-020-00649-5.

Hovland, M., & Sommerville, J. H., 1985. Characteristics of two natural gas seepages in the North Sea. *Marine and Petroleum Geology*, *2*(4), 319-326.

Hovland, M., & Judd, A. G., 1988. *Seabed pockmarks and seepages: impact on geology, biology and the marine environment* (Vol. 293). London: Graham & Trotman.

Hovland, M. & Svensen, H., 2006. Submarine pingoes: Indicators of shallow gas hydrates in a pockmark at Nyegga, Norwegian Sea. Marine Geology 228 (1-4), 15-23.ISSN 0025-3227. https://doi.org/10.1016/j.margeo.2005.12.005.

James, R. H., Bousquet, P., Bussmann, I., et al., 2016. Effects of climate change on methane emissions from seafloor sediments in the Arctic Ocean: A review. Limnology and Oceanography, 61(S1), S283–S299. Portico. https://doi.org/10.1002/lno.10307.

Judd, A.G., 2004. Natural seabed gas seeps as sources of atmospheric methane. Env Geol 46**,** 988–996. https://doi.org/10.1007/s00254-004-1083-3.

Kannberg, P. K., Tréhu, A. M., Pierce, S. D., et al., 2013. Temporal variation of methane flares in the ocean above Hydrate Ridge, Oregon. Earth and Planetary Science Letters, 368, 33–42. https://doi.org/10.1016/j.epsl.2013.02.030

Kennett, J. P., Cannariato, K. G., Hendy, I. L., et al., 2000. Carbon isotopic evidence for methane hydrate instability during Quaternary interstadials. Science 288(5463), 128-133, https://doi.org/10.1126/science.288.5463.128.

Kennett, J. P., Cannariato, K. G., Hendy, I. L., et al., 2003. Methane Hydrates in Quaternary Climate Change: the Clathrate Gun Hypothesis. [pp.216] AGU, Washington, D.C.

Krieger, K. J., 2002. Coral (Primnoa) impacted by fishing gear in the Gulf of Alaska. In Willison, J. H. M., J. Hall, S. E. Gass, E. L. R. Kenchington, P. Doherty & M. Butler (eds), Proceedings of the First International Symposium on Deep Sea Corals. Ecology Action Center, Halifax, Canada: in press.

Lammers, S., Suess, E., Hovland, M., 1995. A large methane plume east of Bear Island (Barents Sea): implications for the marine methane cycle. Geol. Rundsch 84(1), 59-66. https://doi.org/10.1007/BF00192242.

Lashof, D. A., Ahuja, D. R., 1990. Relative contributions of green-house gas emissions to global warming. Nature 344, 529– 531.

Lee, Y.B., Hautala, S.L., 2021. Understanding the Long-Term Tidal Modulation on Methane Bubble Emissions Using Acoustics, Southern Hydrate Ridge, Cascadia. Journal of Advanced Geospatial and Science Technology. 1(1), 70-88.

Lessard-Pilon, S., Porter, M. D., Cordes, E. E., et al., 2010. Community composition and temporal change at deep Gulf of Mexico cold seeps. Deep Sea Research Part II: Topical Studies in Oceanography, 57(21–23), 1891–1903. https://doi.org/10.1016/j.dsr2.2010.05.012.

Levin, L. A., Mendoza, G. F., Grupe, B. M., et al., 2015. Biodiversity on the Rocks: Macrofauna Inhabiting Authigenic Carbonate at Costa Rica Methane Seeps. PLoS ONE 10(7): e0131080. https://doi.org/10.1371/journal.pone.0131080 PMID: 26158723.

Lind, S., Ingvaldsen, R. G., Furevik, T. 2018. Arctic warming hotspot in the northern Barents Sea linked to declining sea-ice import. Nature Climate Change 8(7), 634-639, https://doi.org/10.1038/s41558-018-0205-y.

Lösekann, T., Robador, A., Niemann, H., et al., 2008. Endosymbioses between bacteria and deep-sea siboglinid tubeworms from an Arctic Cold Seep (Haakon Mosby Mud Volcano, Barents Sea). Environmental Microbiology 10: 3237-3254. https://doi.org/10.1111/j.1462-2920.2008.01712.x.

Lundschien, B. A., Høy, T., Mørk, A., 2014. Triassic hydrocarbon potential in the Northern Barents Sea; integrating Svalbard and stratigraphic core data. Norwegian Petroleum Directorate Bulletin 11, 3–20.

Luo, M., Dale, A. W., Haffert, L., Haeckel, M., Koch, S., Crutchley, G., ... & Greinert, J. (2016). A quantitative assessment of methane cycling in Hikurangi Margin sediments (New Zealand) using geophysical imaging and biogeochemical modeling. *Geochemistry, Geophysics, Geosystems*, *17*(12), 4817-4835.

MacDonald, G.J., 1990. Role of methane clathrates in past and future climates. Climatic Change 16, 247–281. https://doi.org/10.1007/BF00144504.

März, C., Hoffmann, J., Bleil, U., et al., 2008. Diagenetic changes of magnetic and geochemical signals by anaerobic methane oxidation in sediments of the Zambezi deep-sea fan (SW Indian Ocean). Marine Geology 255(3-4): 118-130.

Nixon, F. C., Chand, S., Thorsnes, T., et al., 2019. A modified gas hydrate-geomorphological model for a new discovery of enigmatic craters and seabed mounds in the Central Barents Sea, Norway. Geo-Marine Letters, 39, 191-203.

O'Connor, F. M., Boucher, O., Gedney, N., et al., 2010. Possible role of wetlands, permafrost and methane hydrates in the methane cycle under future climate change: A review. Rev. Geophys. 48, RG4005, https://doi.org/10.1029/2010RG000326.

Onarheim, I. H., Årthun, M., 2017. Toward an ice-free Barents Sea. Geophys. Res. Lett. 44, 2017GL074304, https://doi.org/10.1002/2017GL074304, 2017.

Pasulka, A. L., Goffredi, S. K., Tavormina, P. L., et al., 2017. Colonial Tube-Dwelling Ciliates Influence Methane Cycling and Microbial Diversity within Methane Seep Ecosystems. Frontiers in Marine Science, 3. https://doi.org/10.3389/fmars.2016.00276.

Parmentier, F., Christensen, T., 2013. Arctic: Speed of methane release. Nature 500, 529. https://doi.org/10.1038/500529a.

Pereira, O. S., Gonzalez, J., Mendoza, G. F., et al., 2021. The dynamic influence of methane seepage on macrofauna inhabiting authigenic carbonates. Ecosphere, 12(10). Portico. https://doi.org/10.1002/ecs2.3744.

Pimenov, N.V., Savvichev, A. S., Rusanov, I. I. et al., 2000. Microbiological Processes of the Carbon and Sulfur Cycles at Cold Methane Seeps of the North Atlantic. Microbiology 69**,** 709–720. https://doi.org/10.1023/A:1026666527034.

Platt, S.M., Eckhardt, S., Ferré, B., et al., 2018. Methane at Svalbard and over the European Arctic Ocean. Atmospheric Chemistry and Physics 18, 17207-17224, https://doi.org/10.5194/acp-18-17207-2018.

Rajan, A., Mienert, J., Bünz, S., 2012. Acoustic evidence for a gas migration and release system in Arctic glaciated continental margins offshore NW-Svalbard. Marine and Petroleum Geology 32(1): 36-49, ISSN 0264-8172, https://doi.org/10.1016/j.marpetgeo.2011.12.008.

Rehder, G., Keir, R. S., Suess, E., et al. 1998. The Multiple Sources and Patterns of Methane in North Sea Waters. Aquatic Geochemistry 4**,** 403–427. https://doi.org/10.1023/A:1009644600833.

Reigstad, M., Carroll, J., Slagstad, D., et al., 2011. Intra-regional comparison of productivity, carbon flux and ecosystem composition within the northern Barents Sea. *Progress in Oceanography*, *90*(1-4), 33-46.

Ritt, B., Pierre, C., Gauthier, O., et al., 2011. Diversity and distribution of cold-seep fauna associated with different geological and environmental setttings at mud volcanoes and pockmarks of the Nike Deep-Sea Fan. Mar. Biol. 158, 1187–1210. https://doi.org/10.1007/s00227-011-1679-6.

Roark, E. B., Guilderson, T. P., Dunbar, R. B., Fallon, S. J., & Mucciarone, D. A. 2009. Extreme longevity in proteinaceous deep-sea corals. Proceedings of the National Academy of Sciences, 106(13), 5204–5208. https://doi.org/10.1073/pnas.0810875106.

Roberts, J. M., Wheeler, A., Freiwald, A., & Cairns, S., 2009. Cold-water corals: the biology and geology of deep-sea coral habitats. Cambridge University Press.

Roberts, M. 2013. Cold-water coral reefs. In S. A. Elias (Ed.), Reference Module in Earth Systems and Environmental Sciences Elsevier. https://doi.org/10.1016/B978-0-12-409548-9.04041-0.

Römer, M., Riedel, M., Scherwath, M., Heesemann, M., & Spence, G. D., 2016. Tidally controlled gas bubble emissions: A comprehensive study using long-term monitoring data from the NEPTUNE cabled observatory offshore Vancouver Island. *Geochemistry*, *Geophysics*, *Geosystems*, *17*(9), 3797-3814.

Ruppel, C., 2011. Methane hydrates and the future of natural gas. Supplementary Paper #4, The Future of Natural Gas, MIT Energy Initiative study, 25 pp. Staff (5 April 2011) World Shale Gas Resources: An Initial Assessment of 14 Regions Outside the United States US Energy Information Administration, Analysis and Projections, Received 26 August 2012.

Ruppel, C. D., & Kessler, J. D., 2017. The interaction of climate change and methane hydrates. Rev. Geophys. 55, 126- 168, https://doi.org/:10.1002/2016RG000534.

Sahling, H., Römer, M., Pape, T., et al., 2014. Gas emissions at the continental margin west of Svalbard: mapping, sampling and quantification. Biogeosciences 11(21), 6029-6046, https://doi.org/10.5194/bg-11-6029-2014.

Sarkar, S., Berndt, C., Minshull, T. A., et al., 2012. Seismic evidence for shallow gas-escape features associated with a retreating gas hydrate zone offshore west Svalbard. Journal of Geophysical Research: Solid Earth 117: B9. https://doi.org/10/1029/2011JB009126.

Sen, A., Åstrom, E. K. L., Hong, W. L., et al., 2018. Geophysical and geochemical controls on the megafaunal community of a high Arctic cold seep. Biogeosciences, 15(14), 4533-4559, https://doi.org/10.5194/bg-15-4533-2018.

Serov, P., Vadakkepuliyambatta, S., Mienert, J., et al., 2017. Postglacial response of Arctic Ocean gas hydrates to climatic amelioration. *Proceedings of the National Academy of Sciences*, *114*(24), 6215-6220.

Shakhova, N., Semiletov, I., Leifer, I., et al. 2014. Ebullition and storm-induced methane release from the East Siberian Arctic Shelf. Nature Geosci. 7, 64–70. https://doi.org/10.1038/ngeo2007.

Smith, A. J., Mienert, J., Bűnz, S., 2014. Thermogenic methane injection via bubble transport into the upper Arctic Ocean from the hydrate-charged Vestnesa Ridge, Svalbard. AGU 15(5): 1945-1959. https://doi.org/10/1002/2013GC005179.

Southward, E. C., 1982. Bacterial Symbionts in Pogonophora. J. Mar. Biol. Assoc. U. K. 62(4), 889-906, https://doi.org/10.1017//S0025315400044131, 1982.

Southward, E. C., Schulze, A., Gardiner, S. L., 2005. Pogonophora (Annelida): form and function. Hydrobiologia 535/536, 227-251, 2005.

Spielhagen, R. F., Werner, K., Sørensen, S. A., et al., 2011. Enhanced Modern Heat Transfer to the Arctic by Warm Atlantic Water. Science 331(6), 450-, https://doi.org/:10.1126/science.1197397.

Suess, E. (2014). Marine cold seeps and their manifestations: geological control, biogeochemical criteria and environmental conditions. International Journal of Earth Sciences, 103(7), 1889–1916. https://doi.org/10.1007/s00531-014-1010-0.

Thatcher, K. E., Westbrook, G. K., Sarkar, S., et al., 2013. Methane release from warming-induced hydrate dissociation in the West Svalbard continental margin: Timing, rates, and geological controls. Journal of Geophysical Research: Solid Earth 118(1), 22-38, https://doi.org/10.1029/2012JB009605.

Torres, M. E., McManus, J., Hammond, D. E., et al., 2002. Fluid and chemical fluxes in and out of sediments hosting methane hydrate deposits on Hydrate Ridge, OR, I: Hydrological provinces. *Earth and Planetary Science Letters*, *201*(3-4), 525-540.

Tryon, M. D., Brown, K. M., & Torres, M. E., 2002. Fluid and chemical flux in and out of sediments hosting methane hydrate deposits on Hydrate Ridge, OR, II: Hydrological processes. Earth and Planetary Science Letters, 201(3–4), 541–557. https://doi.org/10.1016/s0012-821x(02)00732-x.

Ussler III, W., Paull, C. K., 2008. Rates of anaerobic oxidation of methane and authigenic carbonate mineralization in methane-rich deep-sea sediments inferred from models and geochemical profiles. Earth and Planetary Science Letters 266(3–4): 271-287.

Waage, M., Serov, P., Andreassen, K., et al., 2020. Geological controls of giant crater development on the Arctic seafloor. *Scientific reports*, *10*(1), 1-12.

Waller, R., Watling, L., Auster, P., et al., 2007. Fisheries impacts on the Corner Rise Seamounts. Journal of the Marine Biological Association of the UK 87:1075-1076.

Weniger, P., Blumenberg, M., Berglar, K., et al., 2019. Origin of near-surface hydrocarbon gases bound in northern Barents Sea sediments. Marine and Petroleum Geology 102, 455-476.

Weslawski, J. M., Kendall, M. A., Wlodarska-Kowalczuk, M., et al., 2011. Climate change effects on Arctic fjord and coastal macrobenthic diversity-observations and predictions. Mar. Biodivers. 41, 71-85, https://doi.org/10.1007/s12526-010-0073-9.

Westbrook, G. K., Thatcher, K. E., Rohling, E. J., et al., 2009. Escape of methane gas from the seabed along the West Spitsbergen continental margin. Geophysical Research Letters 36(15) https://doi.org/10.1029/2009GL039191.

Zeppilli, D., Canals, M., Danovaro, R., 2012. Pockmarks enhance deep-sea benthic biodiversity: a case study in the western Mediterranean Sea. Diversity and Distributions 18(8): 832-846, https://doi.org/10.1111/j.1472-4642.2011.00859.x.

Figures

Figure 1. Regional map indicating the Storbanken Crater site along the Norwegian continental shelf and Barents Sea region, between the Isfjorden and Kongsfjorden cross-shelf troughs. The Polar Stern, Prins Karls Forland and Pingo sites are also noted. Seafloor physical and chemical habitats and benthic community structure of the Storbanken area east of Svalbard in the Barents Sea was investigated June 21 – July 03, 2017 (120 - 300 m depth).

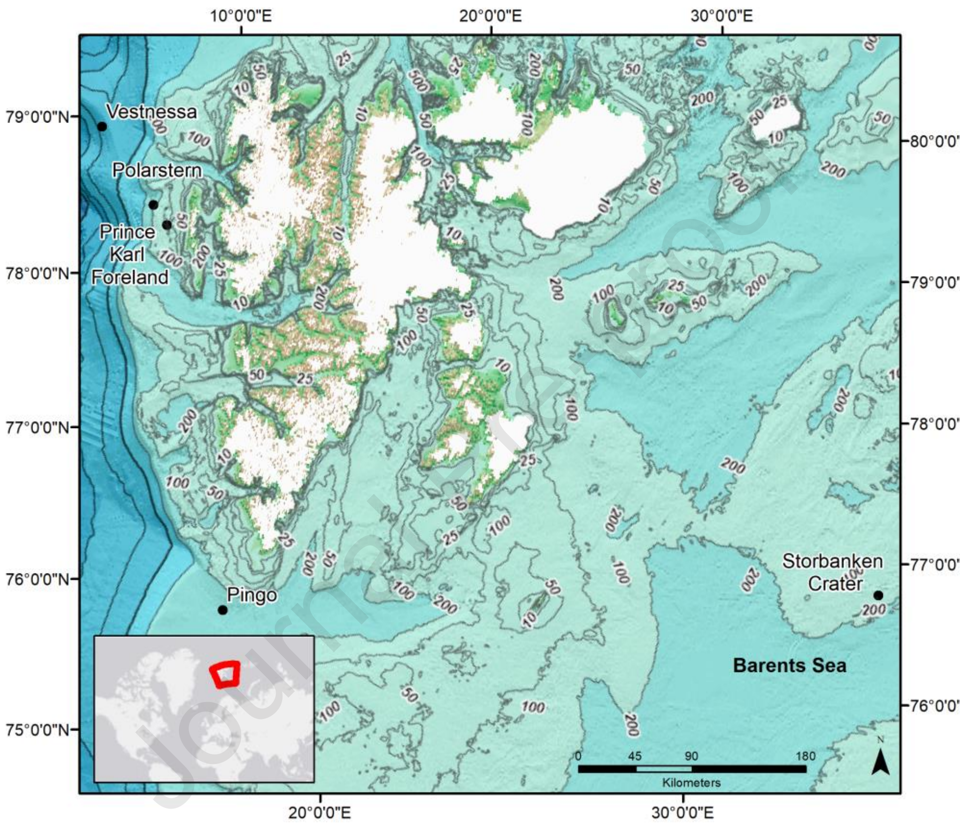

Figure 2A. Parts of seismic-profile NPD1204RE15-108 crossing the southern parts of Storbanken. The geological structure is a large complex anticlinal feature, eroded at the crest, and highly faulted by faults going all the way down to Permian-Carboniferous strata. The most likely potential source rock intervals are in the Olenekian, Anisian and Ladinian sequences of Lower to Middle Triassic age. The seafloor in the crater area consists mostly of sub-cropping Uppermost Triassic to Jurassic layers, with very little soft sediments on top (below seismic resolution). Twt = Two-way-travel time.

Figure 2B. Parts of seismic-profile NPD1204RE15-220 crossing the western parts of the Storbanken site. The profile shows a faulted and eroded anticline with gas leaking into the water column at the seafloor related to faults at the top of the eroded structure. Bright amplitudes, interpreted as increased levels of gas in the sedimentary layers, are observed in several places related to the faults. A possible cross-cutting bottom simulating reflector (BSR) is observed at the top of the structure. Twt = Two-way-travel time.

(A)

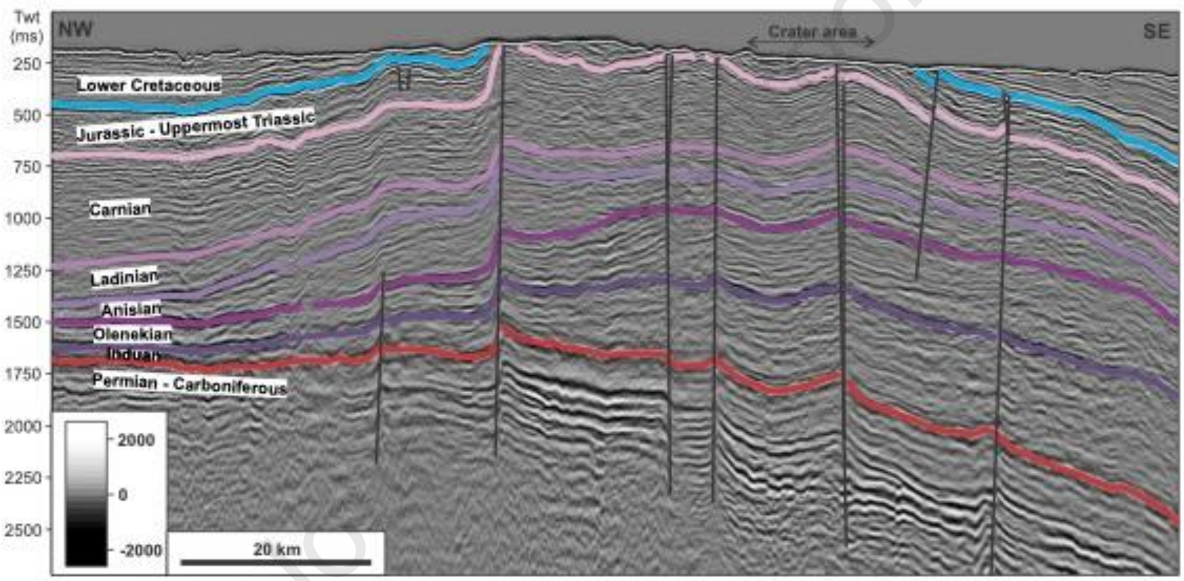

(B)

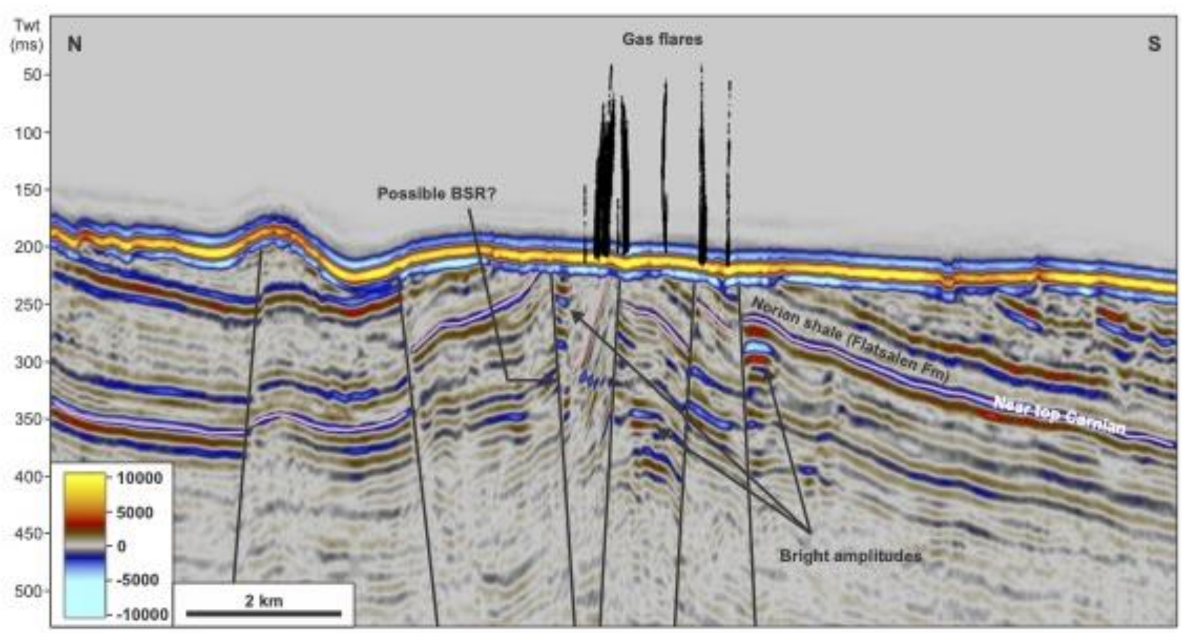

Figure 3. *TowCam* seafloor imaging and sampling system was used to provide geographically referenced imagery to investigate geological characteristics, habitat and biological communities. A total of 6,827 images and 40 sediment multicore samples from 14 seafloor surveys were obtained within the Storbanken Crater site. (A) Vehicle shown here with sediment multi-core samples during the CAGE 17-2 cruise. (B) Example of a post multi-core sampling event, showing the individual core holes, imprint of *TowCam* frame, and 20cm laser-scale.

(A)

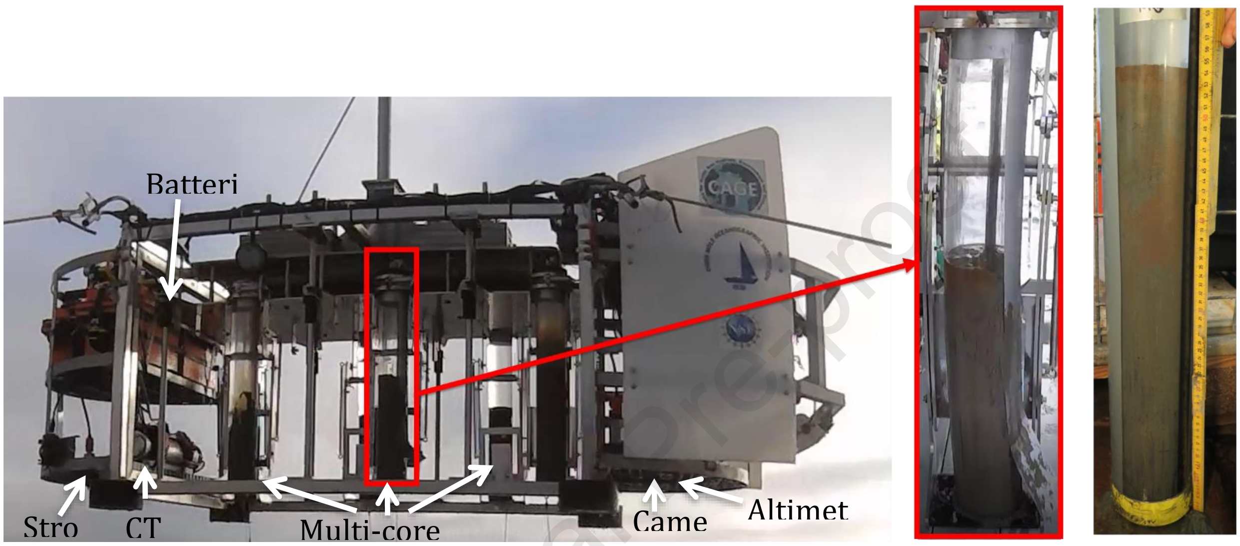

(B)

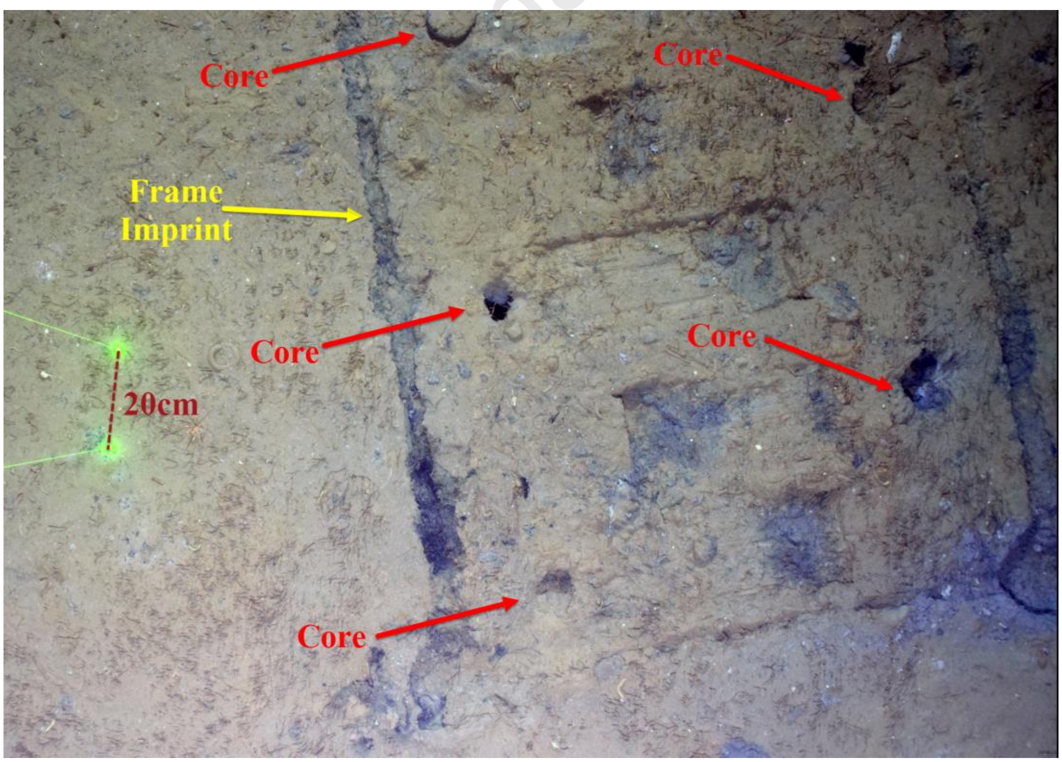

Figure 4. Ship-based water-column imaging of methane plumes via multibeam echosounder show differences in strength and locations of plumes between co-located surveys in 2015 (blue) and 2017 (red).

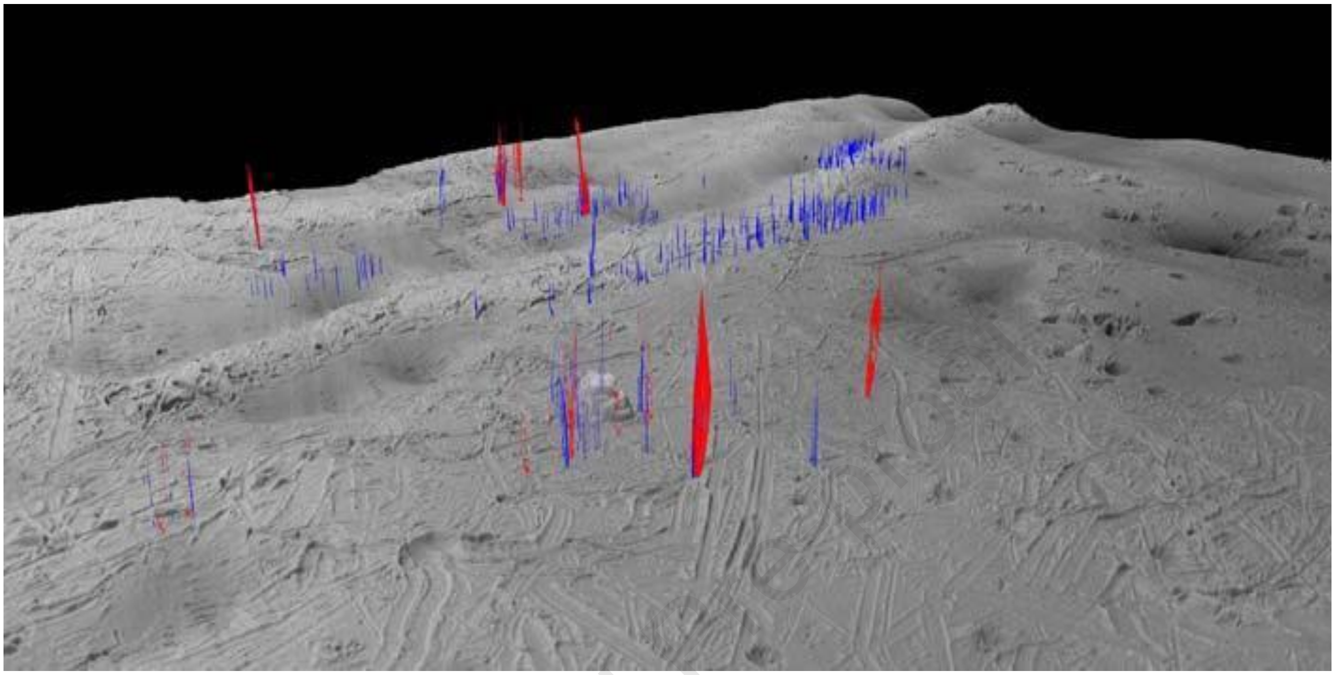

Figure 5. The location of *TowCam* survey sites in the Storbanken Crater area. Green circles indicate seafloor survey locations and numbers indicate the towed survey ID as presented in Table 1. Purple triangles indicate the location of identified seep sites.

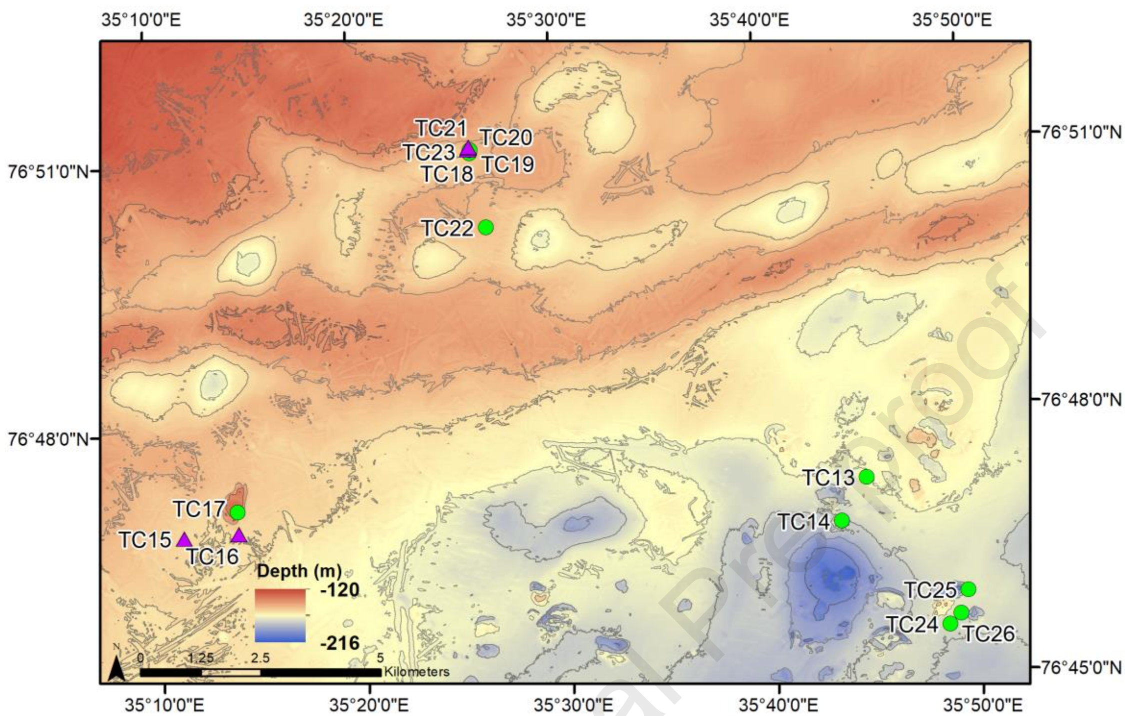

Figure 6. (A) The seafloor habitat classification of *Towcam* images (*TowCam* # HH942-23 shown here), revealed seafloor characteristics (i.e., drop stones, outcrops, sediment, fishing trawl marks) including the locations seafloor expressions of microbial mats (blue circles) within a non-crater site in the Storbanken area. **(B)** A typically observed expression of microbial mat indicating hydrocarbon release (width of mat is ~20 cm). **(C)** Multiple trawl marks (more than 12) were observed along one track line in the non-crater site.

(A) **(B)**

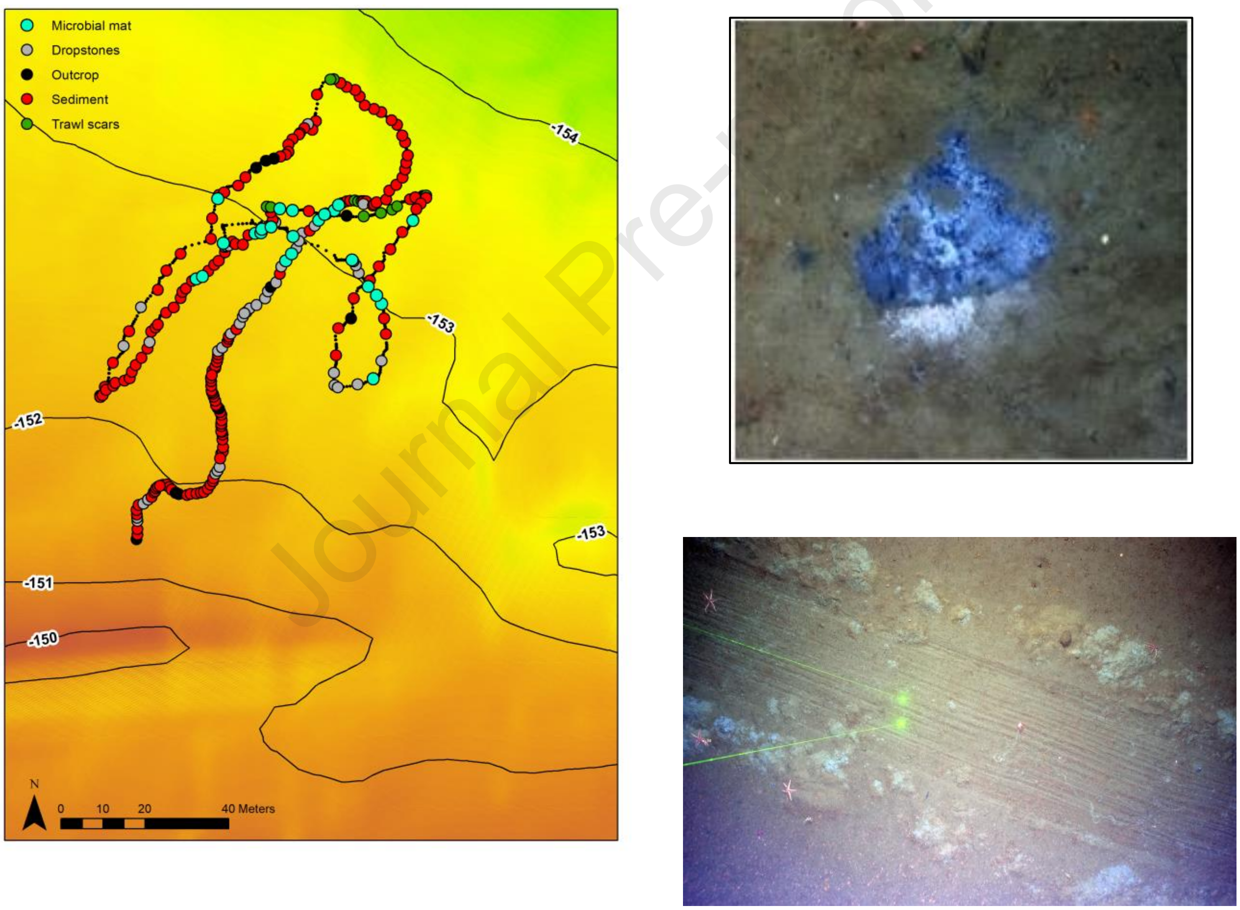

(C)

Figure 7. Representative *TowCam* (TC) images of faunal habitats in the Storbanken area. A) TC-14 Seafloor covered by rocks and other hard substrates with anemones and sponges. B) TC-15 Microbial mat visible, indicating a seep habitat. Brittle stars, and starfish in soft sediment surround the patchy seep. C) TC-16 Patchy microbial mats, with lots of brittle stars and starfish in the sediment. D) TC-17 Rocky outcrops are covered with crinoids. Anemones and sea star also visible. E) TC-18 Patches of microbial mats and potential carbonate crusts colonized muddy seafloor with brittle stars. F) TC-22 Block colonized by sessile organisms including brittle stars, sponges, and crinoids. The horizontal distance across the bottom of each image is approximately 3 to 4 meters while 20 cm distance between the green parallel lasers. Yellow arrows indicate microbial mats.

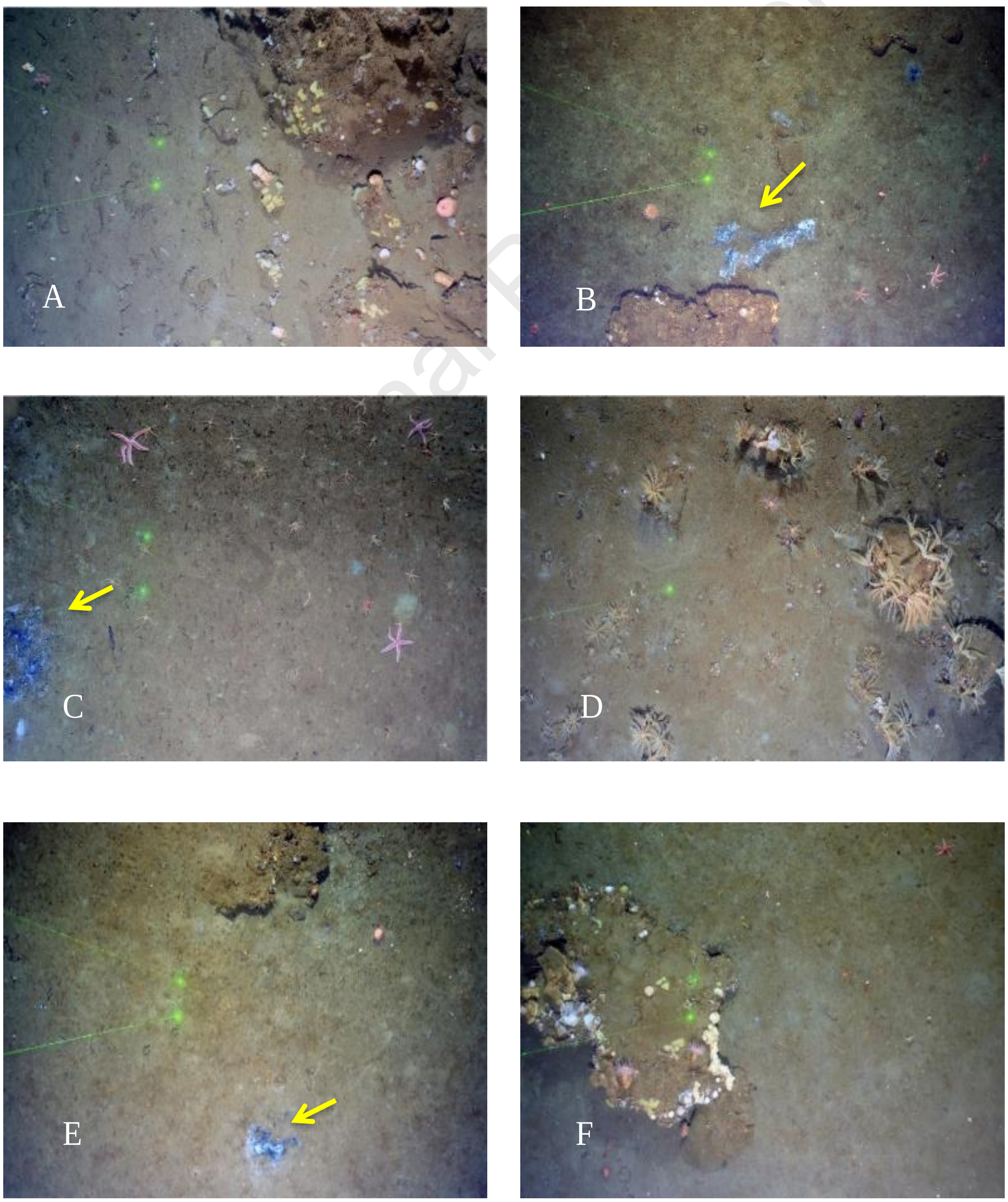

Figure 8A. The composition and distribution of biological community features outside the crater site (*TowCam* # HH942-23) within the Storbanken area. More than 16 megafaunal taxa were observed over 3 km of seafloor at the non-crater site. Fauna included multiple species of encrusting sponge, fish including schooling fish, soft corals, stalked crinoids, anemones, brittle stars, sea stars and psolid sea cucumbers**.**

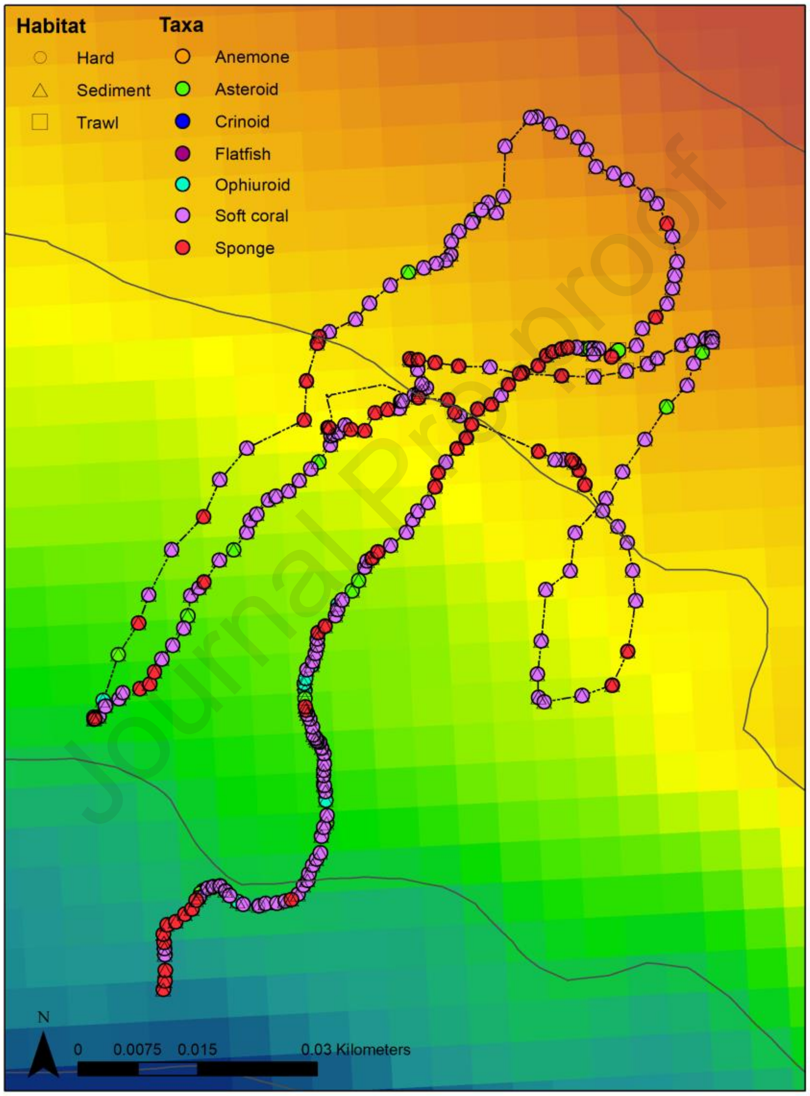

966 **Figure 8B.** The composition and distribution of biological community features inside the crater site (*TowCam* #
967 HH942-25) within the Storbanken area.

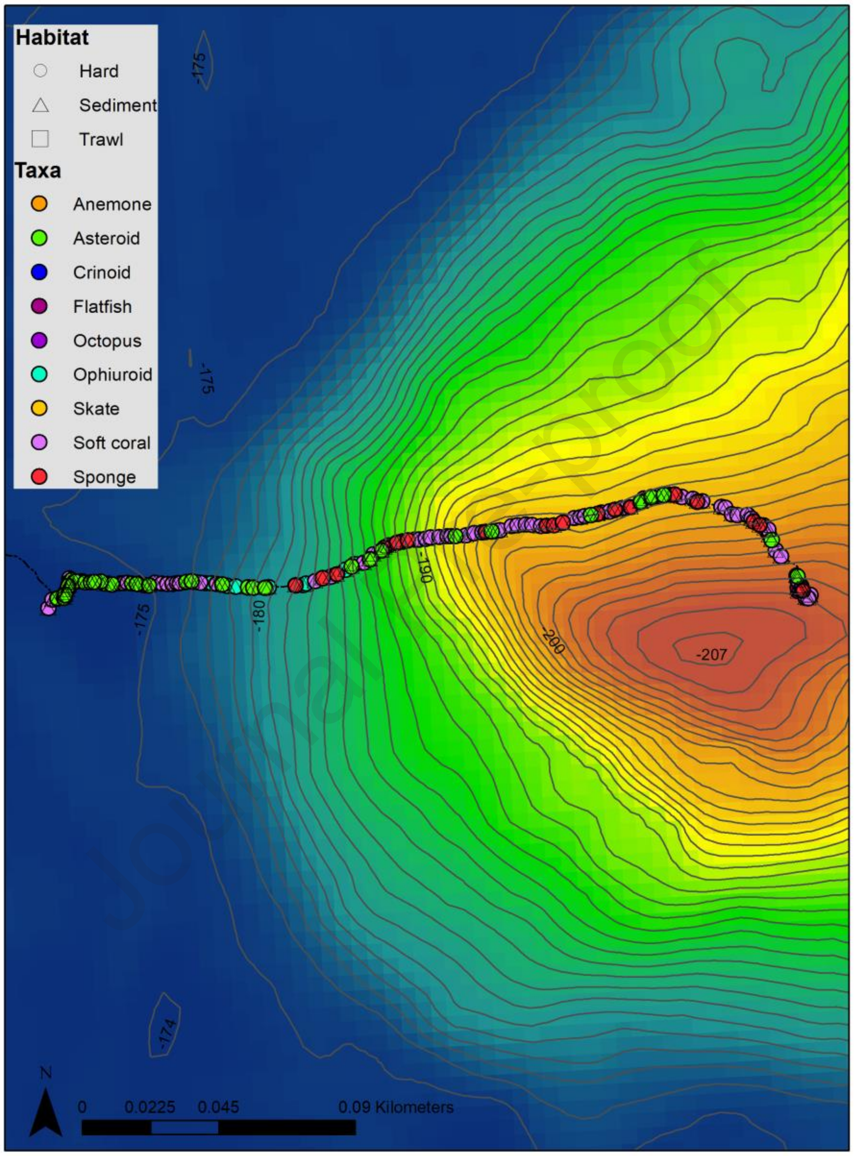

Table 1. Summary of 14 tows of the towed-camera system *TowCam* during cruise HH932 aboard the R/V *Helmer Hanssen* to investigate cold seeps in the Barents Sea in 2017. Green highlight indicates *TowCam* surveys at the crater site.

***TowCam* #**	**Site**	**Latitude**	**Longitude**	**Depth (m)**	**Dominant Seafloor Habitat**
HH932-TC13	1 km NE OBC	76 47.215	35 44.760	160	Soft Sediment
HH933-TC14	OBC-D1	76 46.737	35 43.457	220	Hard substrates
HH939-TC15	OBC-M1	76 46.840	35 11.188	155	Seep
HH940-TC16	OBC-M1	76 46.8657	35 13.895	155	Seep
HH942-TC17	OBC-M1	76 47.115	35 13.856	160	Rocky outcrop
HH947-TC18	OBC-D3	76 51.039	35 25.927	150	Seep and Carbonate crusts
HH948-TC19	OBC-D3	76 51.071	35 25.962	160	Seep and Carbonate crusts
HH950-TC20	OBC-D3	76 51.077	35 25.839	150	Seep
HH951-TC21	OBC-D3	76 51.095	35 25.905	160	Seep
HH957-TC22	OBC-D4	76 50.199	35 26.594	150	Soft Sediment
HH958-TC23	OBC-D3	76 51.104	35 25.893	150	Seep
HH962-TC24	OBC-C1	76 45.528	35 48.522	170	Soft Sediment
HH969-TC25	OBC-C1	76 45.903	35 49.492	200	Soft Sediment
HH970-TC26	OBC-C1	76 45.644	35 49.079	160	Rock

Table 2. Location of multicore (MC) and gravity core (GC) stations, the corresponding *TowCam* surveys and water depth at the sampling sites.

Station	*TowCam* Survey	Depth (m)	Latitude	Longitude	Relative position to Feature
MC-933	TC14	221	76 46.119	35 42.921	Within depression D1
MC-939	TC15	156	76 46.865	35 11.194	Proximal (<3 m) to microbial mat
MC-948	TC19	162	76 51.058	35 25.921	North of mapped MAREANO flare
MC-951	TC21	162	76 51.056	35 25.904	
MC-957	TC22	153	76 50.198	35 26.626	Close to microbial mat
MC-962	TC24	170	76 45.548	35 48.424	Close to mapped MAREANO flare
MC-969	TC25	202	76 45.920	35 48.974	Inside a crater
GC-935		191	76 46.842	35 30.915	Outside depression
GC-971		203	76 45.860	35 43.028	Inside depression (D1)
GC-972		203	76 45.859	35 43.033	Inside depression (D1)

Table 3.

Site	*TowCam* ID	Depth (m)	Microbial Mats	Bryozoa	Cnidaria (cf. *Drifa glomerata)*	Porifera	Arthropoda (shrimp; Caridea/ Dendrobranchia)	Arthropoda (Pycnogonid)	Arthropoda (Pagurid crabs)	Arthropoda (Brachyuran crabs)	Echinodermata (Holothuroidea cf. *Psolus*)	Echinodermata (Comatulid crinoid)	Echinodermata (Ophiuroidea)	Mollusca (Gastropod snails)	Mollusca (Octopoda)	Fish
1 km NE OBC	TC13	160	-	+	+ +	+ +	+	+ +	-	-	+	-	+ +	-	-	Small morphospecies
OBC-D1	TC14	220	-	+ +	+ +	+ +	+	+ +	-	+	+ +	-	+ +	-	+	cf. *Hippoglosoides platessoides*, large and small size class (schooling)
OBC-M1	TC15-TC17	155-160	+	+	+ +	+ +	-	-	-	-	+ +	+ +	+ +	-	-	cf. *Hippoglosoides platessoides*; small size class; cf. *Gadus mohua*
OBC-D3	TC18-TC21, TC23	150-160	+ +	+	+ +	+ +	-	-	+	-	+ +	+ +	+ +	+ +	-	cf. *Hippoglosoides platessoides*; small size class
OBC-D4	TC22	150	-	+	+ +	+ +	-	-	+	-	+ +	-	+ +	+ +	-	Small size class
OBC-C1	TC24-TC26	160-200	-	+	+ +	+ +	+	+ +	-	+	+ +	-	+ +	-	-	*cf. Hippoglosoides platessoides*; small size class; (schooling)

-	Not observed
+	Present, < than 10 indiv. per site
+ +	Present, > than 10 indiv. per site

Supplemental Material

Figure 1: Pore water concentration profiles of methane, dissolved iron and calcium in the multicores (left column) and gravity cores (right column). Note the different depth scales for the multicore and gravity plots.

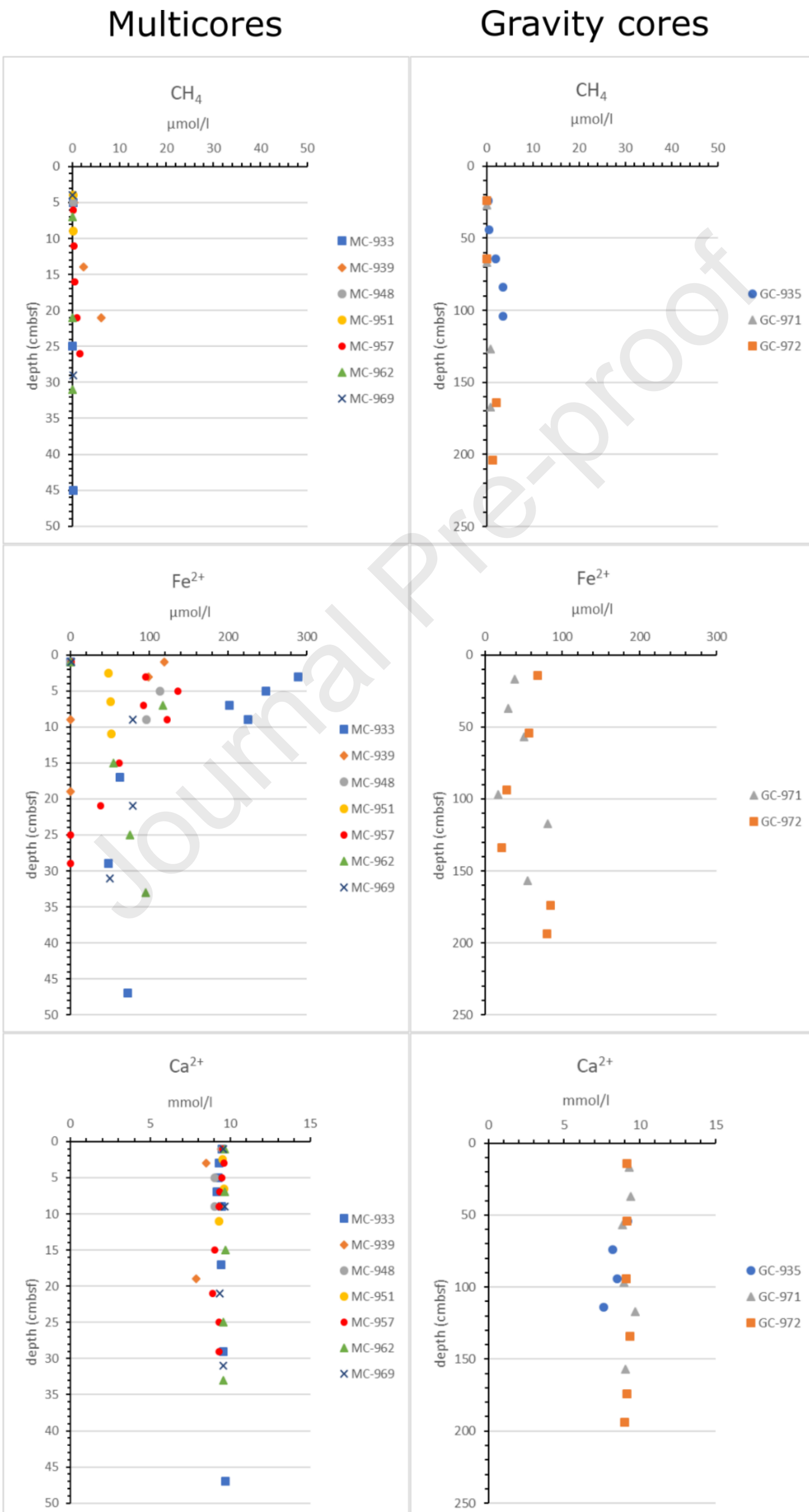

Figure 2: Pore water concentration profiles of strontium and boron in the multicores (left column) and gravity cores (right column). Note the different depth scales for the multicore and gravity plots.

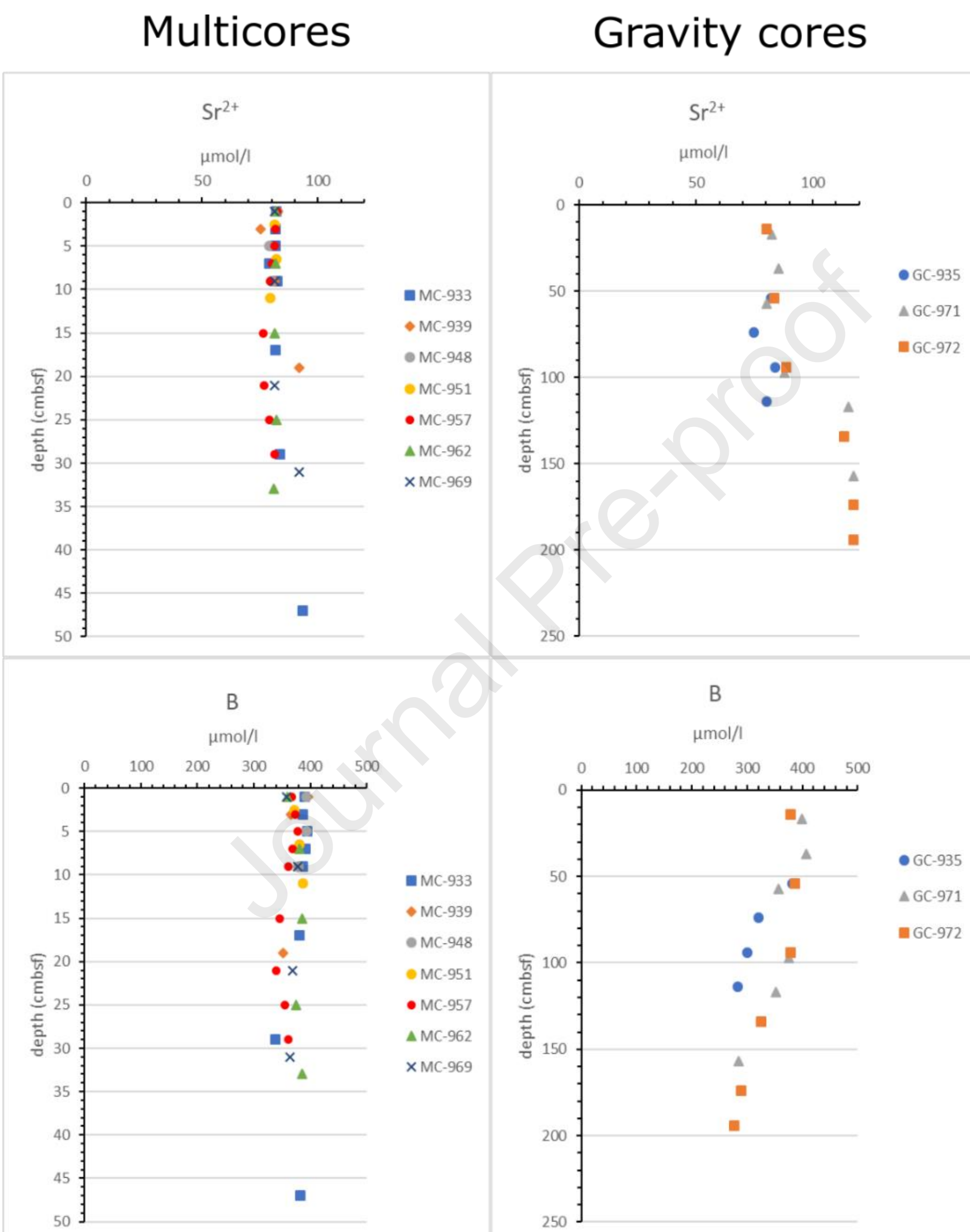

Figure 3: Pore water data of total alkalinity, dissolved inorganic carbon (DIC) and □[13]C-DIC for some of the multicores.

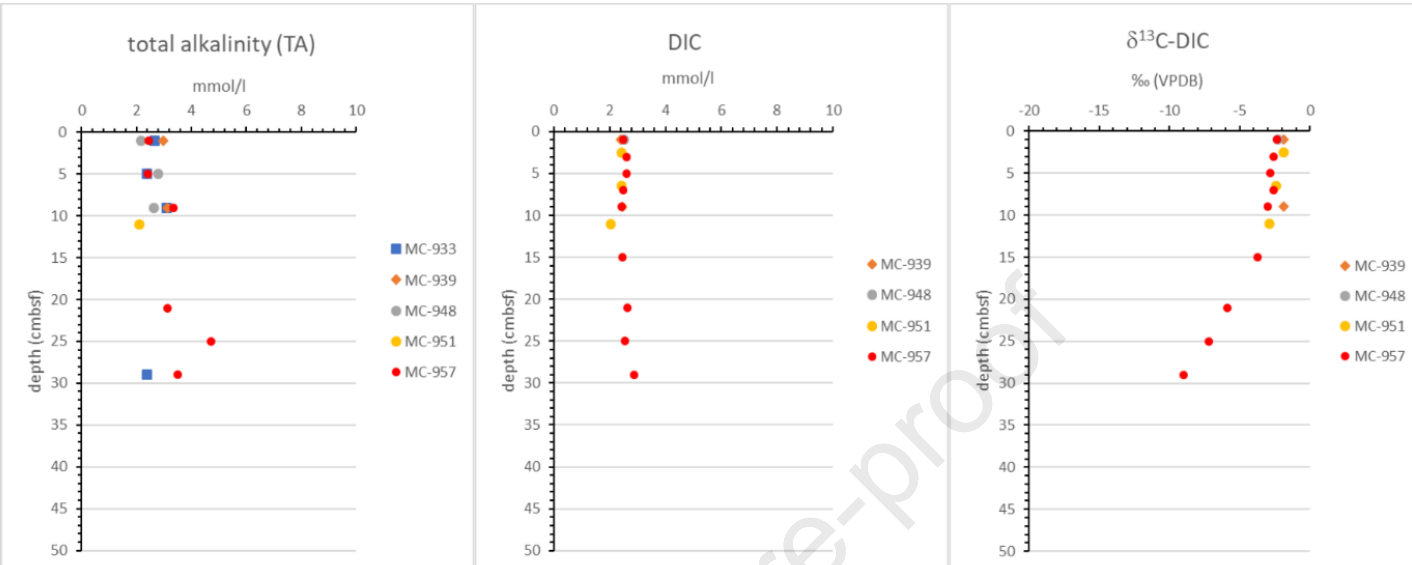

Table 1. Concentration measurements of pore water dissolved components and methane headspace of multicores and gravity cores from cruise CAGE 17-2.

	Depth	Fe^{2+}	Total alkalinity	□^{13}C-DIC	DIC	Ca^{2+}	Sr^{2+}	B	Depth	CH_4
Core	*cm*	*µM*	*mmol/l*	*‰ (VPDB)*	*mmol/l*	*mmol/l*	*µmol/l*	*µmol/l*	*cm*	*µmol/l*
MC-933-5	1	0.0	2.7			9.5	82.1	390.4	5	0.2
	3	288.9				9.3	81.5	387.6	25	0.1
	5	248.2	2.4			9.3	81.7	394.1	45	0.2
	7	201.9				9.2	78.9	391.3		
	9	225.4	3.1			9.5	82.4	386.7		
	17	62.7				9.4	81.5	381.1		
	29	47.9	2.4			9.6	83.4	338.6		
	47	72.3				9.7	93.2	383.0		
GC-935	54		2.5			9.2	82.2	382.1	24	0.4
	74					8.2	74.9	320.1	44	0.5
	94					8.5	83.9	300.6	64	1.9
	114					7.6	80.2	282.1	84	3.5
									104	3.5
MC-939-5	1	119.0	3.0	-1.9	2.4	9.4	82.6	395.9	5	0.4
	3	99.3				8.5	75.2	366.3	14	2.5
	9	0.0	3.1	-1.9	2.5	9.4	81.1	378.4	21	6.1
	19	0.0				7.9	91.9	352.5		
MC-948-2	1	0.4	2.2	-2.3	2.5	9.5	82.4	393.2	5	0.2
	5	113.4	2.8			9.0	79.1	393.2		
	9	96.3	2.6			9.0	79.7	379.3		
MC-951-2	3	48.4		-1.9	2.4	9.5	81.3	371.9	4	0.3
	7	50.9		-2.4	2.4	9.6	82.2	380.2	9	0.1
	11	52.2	2.1	-2.9	2.0	9.3	79.3	386.7		
MC-957-5	1	0.9	2.5	-2.4	2.5	9.5	82.5	367.3	6	0.2
	3	95.4		-2.6	2.6	9.6	81.7	373.7	11	0.4
	5	136.1	2.4	-2.8	2.6	9.5	81.1	377.4	16	0.5
	7	92.9		-2.6	2.5	9.3	80.0	368.2	21	0.9
	9	122.4	3.4	-3.0	2.4	9.3	79.2	360.8	26	1.6
	15	61.6		-3.7	2.4	9.0	76.5	345.1		
	21	38.1	3.1	-5.9	2.6	8.9	76.6	340.4		

	25	0.0	4.7	-7.2	2.5	9.3	79.0	355.2		
	29	0.0	3.5	-9.0	2.9	9.3	81.1	360.8		
MC-962-5	1	0.0				9.7	81.6	359.9	7	0.1
	7	117.3				9.6	81.7	380.2	21	0.1
	15	54.4				9.7	81.4	384.8	31	0.1
	25	75.8				9.6	81.9	374.7		
	33	95.4				9.6	81.0	385.8		
MC-969-5	1	1.3				9.6	81.4	358.0	4	0.1
	9	78.8				9.6	81.3	377.4	29	0.3
	21	79.2				9.4	81.1	369.1		
	31	50.5				9.6	91.8	364.5		
GC-971	17	38.5				9.3	82.6	399.6	27	0.0
	37	30.4				9.4	85.3	407.0	67	0.0
	57	50.1				8.9	80.2	357.1	127	0.9
	97	17.1				8.9	88.0	374.7	167	0.8
	117	80.9				9.7	115.3	351.5		
	157	55.2				9.1	117.6	284.0		
GC-972	14	68.1				9.1	80.2	379.3	24	0.1
	54	57.4				9.1	83.5	385.8	64	0.0
	94	28.3				9.1	88.6	379.3	164	2.1
	134	21.4				9.4	113.4	325.6	204	1.4
	174	85.2				9.2	117.6	288.6		
	194	80.5				9.0	117.6	276.6		

Figures

Figure 1. Regional map indicating the Storbanken Crater site along the Norwegian continental shelf and Barents Sea region, between the Isfjorden and Kongsfjorden cross-shelf troughs. The Polar Stern, Prins Karls Forland and Pingo sites are also noted. Seafloor physical and chemical habitats and benthic community structure of the Storbanken area east of Svalbard in the Barents Sea was investigated June 21 – July 03, 2017 (120 - 300 m depth).

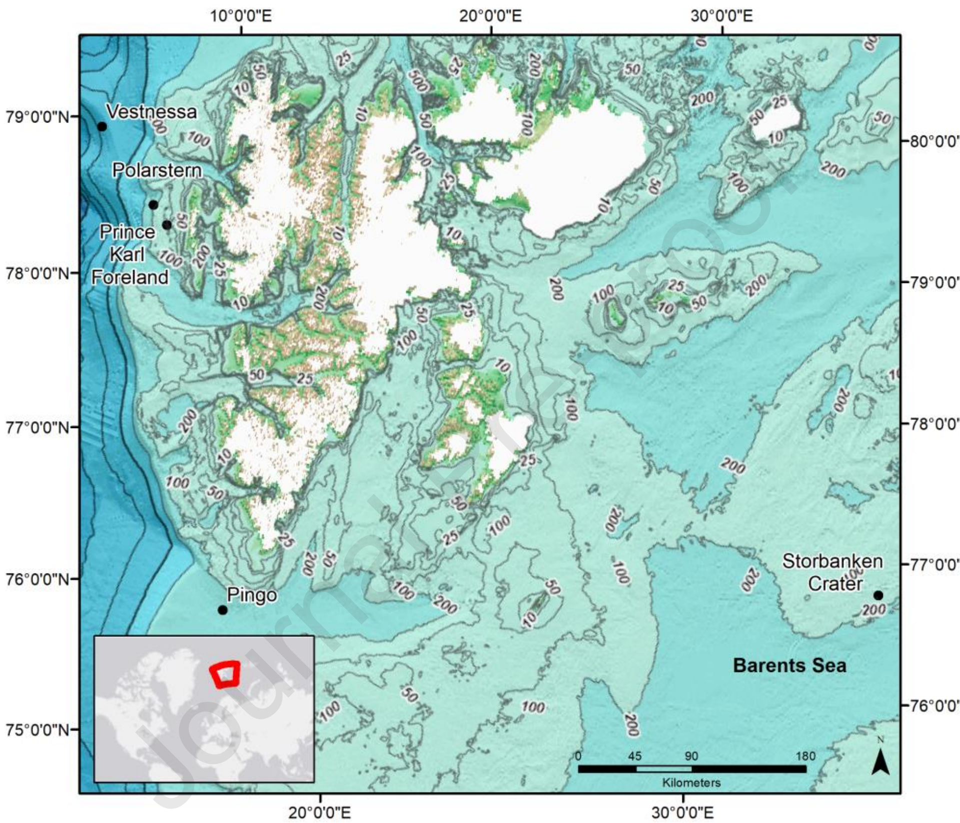

Figure 2A. Parts of seismic-profile NPD1204RE15-108 crossing the southern parts of Storbanken. The geological structure is a large complex anticlinal feature, eroded at the crest, and highly faulted by faults going all the way down to Permian-Carboniferous strata. The most likely potential source rock intervals are in the Olenekian, Anisian and Ladinian sequences of Lower to Middle Triassic age. The seafloor in the crater area consists mostly of sub-cropping Uppermost Triassic to Jurassic layers, with very little soft sediments on top (below seismic resolution). Twt = Two-way-travel time.

Figure 2B. Parts of seismic-profile NPD1204RE15-220 crossing the western parts of the Storbanken site. The profile shows a faulted and eroded anticline with gas leaking into the water column at the seafloor related to faults at the top of the eroded structure. Bright amplitudes, interpreted as increased levels of gas in the sedimentary layers, are observed in several places related to the faults. A possible cross-cutting bottom simulating reflector (BSR) is observed at the top of the structure. Twt = Two-way-travel time.

(A)

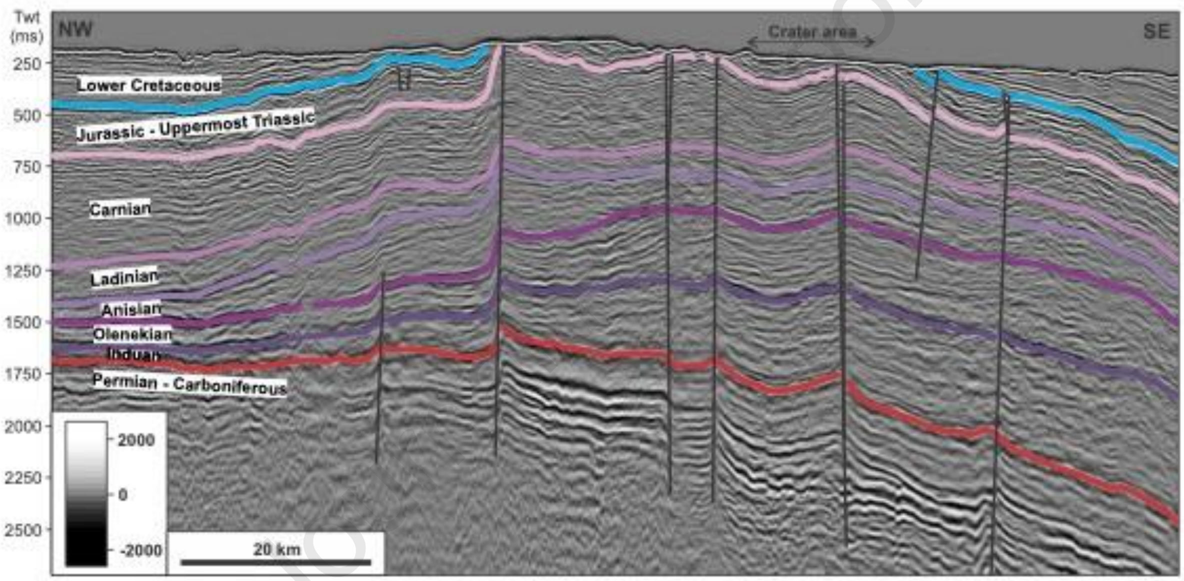

(B)

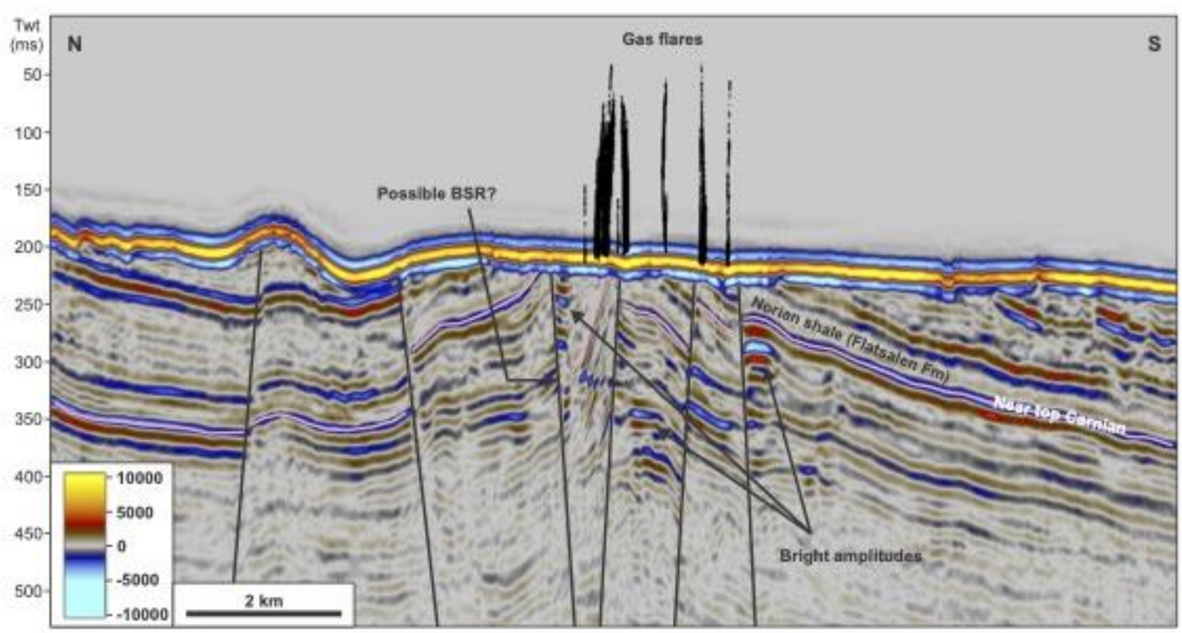

Figure 3. *TowCam* seafloor imaging and sampling system was used to provide geographically referenced imagery to investigate geological characteristics, habitat and biological communities. A total of 6,827 images and 40 sediment multicore samples from 14 seafloor surveys were obtained within the Storbanken Crater site. (A) Vehicle shown here with sediment multi-core samples during the CAGE 17-2 cruise. (B) Example of a post multi-core sampling event, showing the individual core holes, imprint of *TowCam* frame, and 20cm laser-scale.

(A)

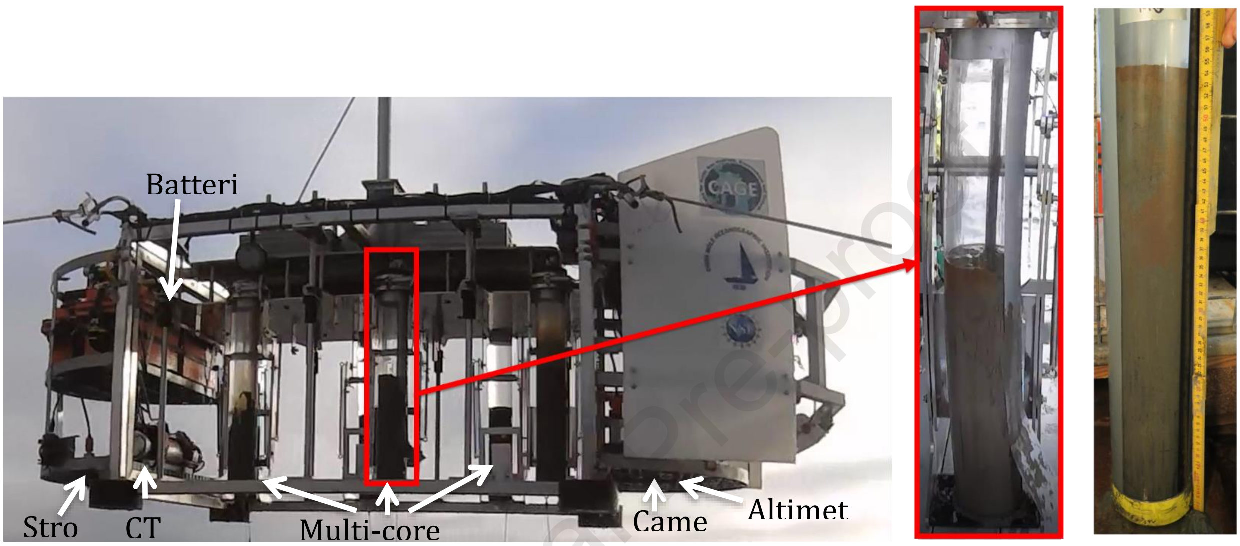

(B)

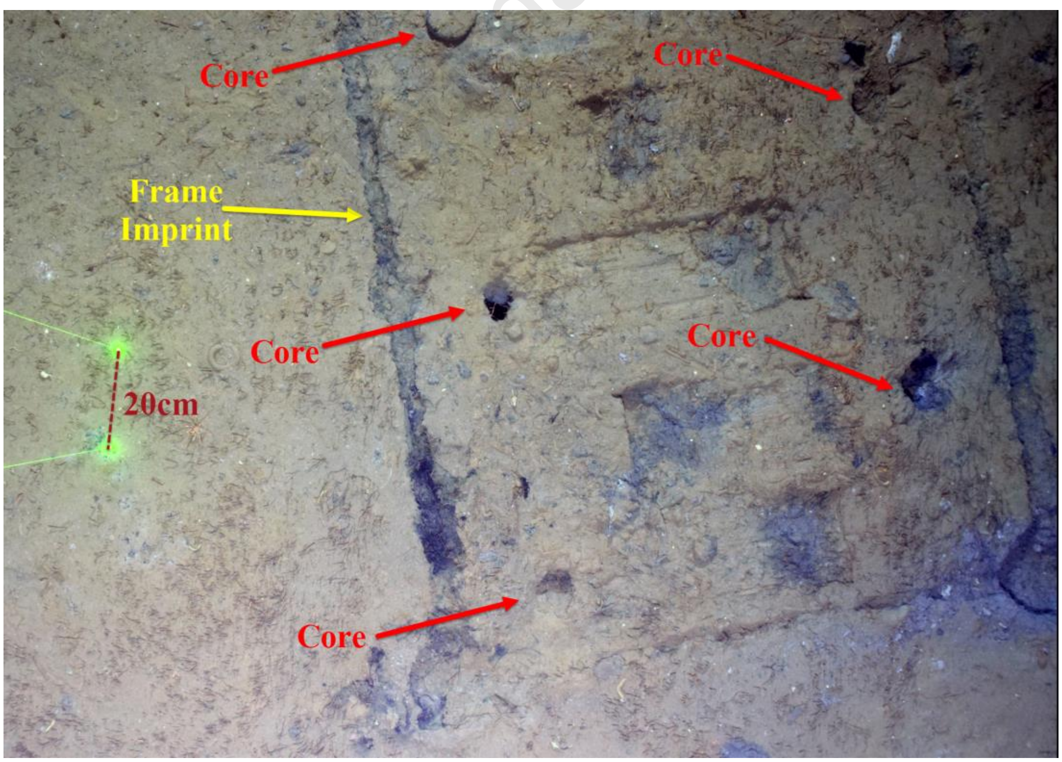

Figure 4. Ship-based water-column imaging of methane plumes via multibeam echosounder show differences in strength and locations of plumes between co-located surveys in 2015 (blue) and 2017 (red).

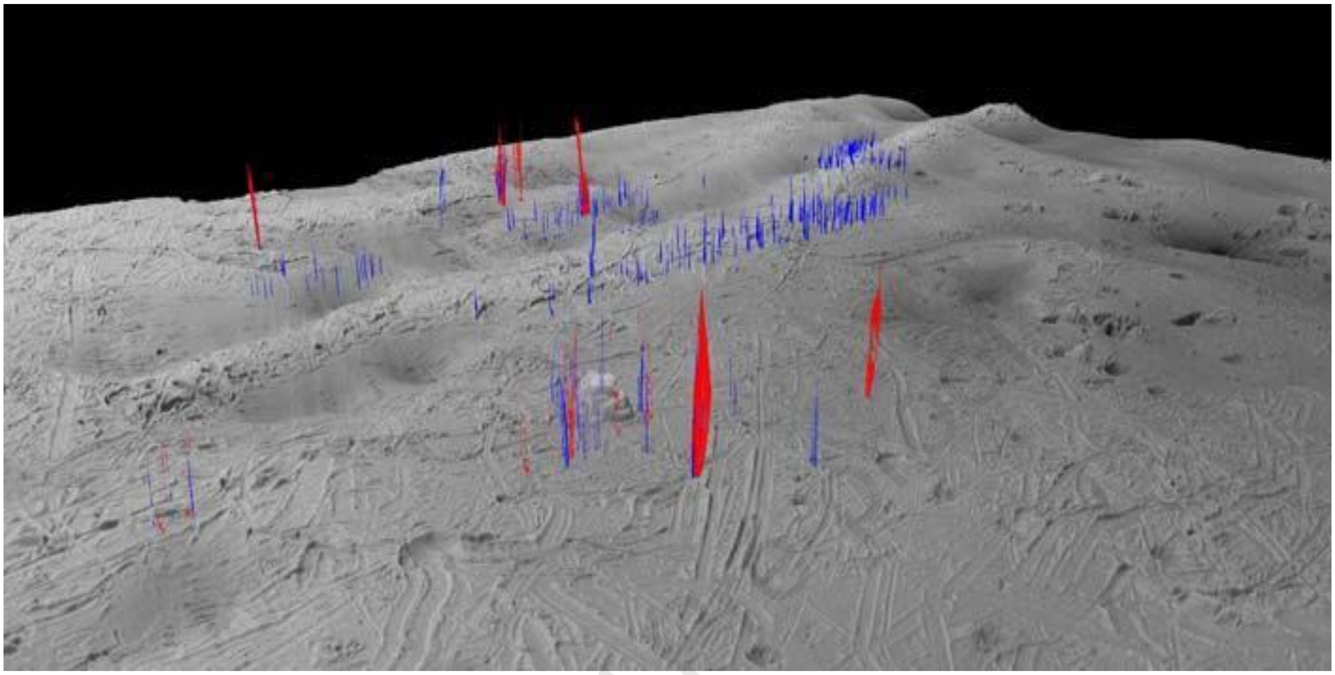

Figure 5. The location of *TowCam* survey sites in the Storbanken Crater area. Green circles indicate seafloor survey locations and numbers indicate the towed survey ID as presented in Table 1. Purple triangles indicate the location of identified seep sites.

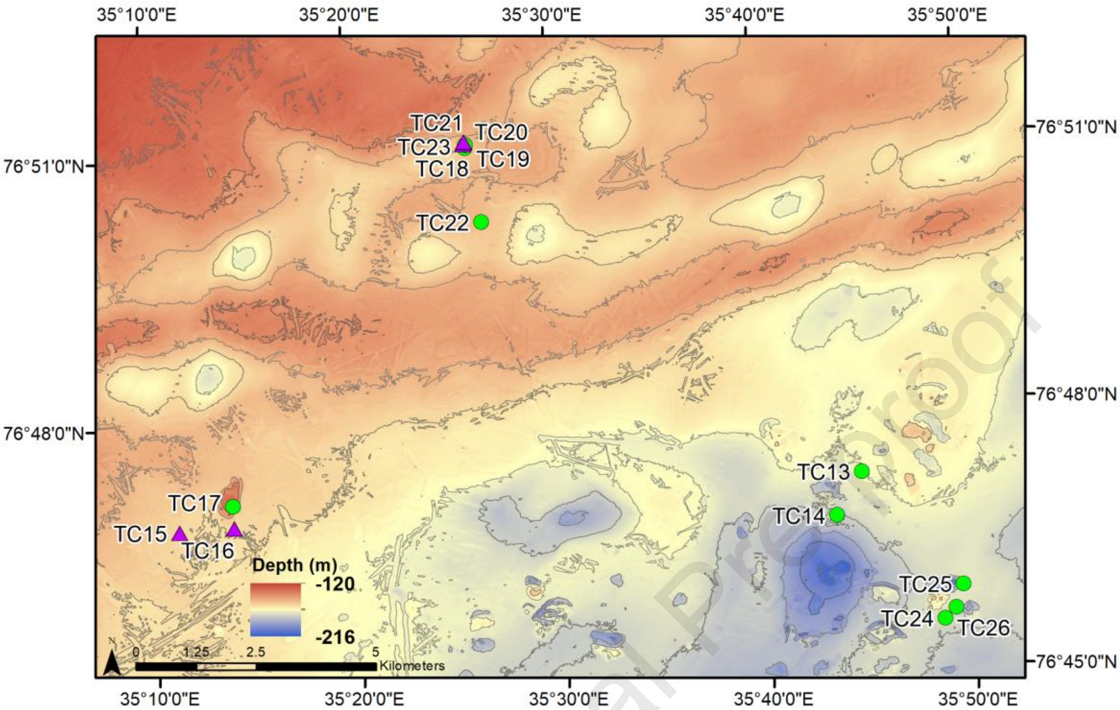

Figure 6. (A) The seafloor habitat classification of *Towcam* images (*TowCam* # HH942-23 shown here), revealed seafloor characteristics (i.e., drop stones, outcrops, sediment, fishing trawl marks) including the locations seafloor expressions of microbial mats (blue circles) within a non-crater site in the Storbanken area. **(B)** A typically observed expression of microbial mat indicating hydrocarbon release (width of mat is ~20 cm). **(C)** Multiple trawl marks (more than 12) were observed along one track line in the non-crater site.

(A) **(B)**

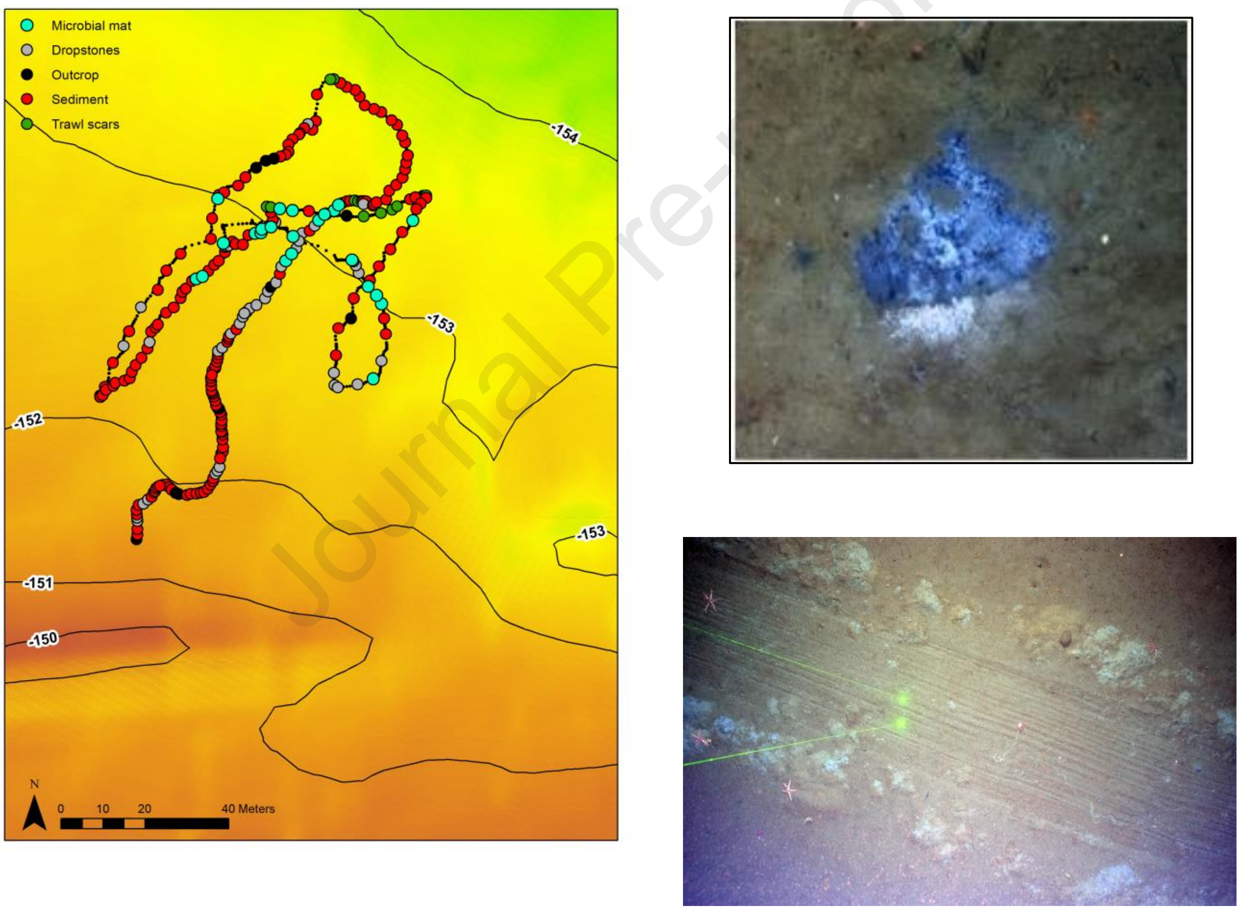

(C)

Figure 7. Representative *TowCam* (TC) images of faunal habitats in the Storbanken area. A) TC-14 Seafloor covered by rocks and other hard substrates with anemones and sponges. B) TC-15 Microbial mat visible, indicating a seep habitat. Brittle stars, and starfish in soft sediment surround the patchy seep. C) TC-16 Patchy microbial mats, with lots of brittle stars and starfish in the sediment. D) TC-17 Rocky outcrops are covered with crinoids. Anemones and sea star also visible. E) TC-18 Patches of microbial mats and potential carbonate crusts colonized muddy seafloor with brittle stars. F) TC-22 Block colonized by sessile organisms including brittle stars, sponges, and crinoids. The horizontal distance across the bottom of each image is approximately 3 to 4 meters while 20 cm distance between the green parallel lasers. Yellow arrows indicate microbial mats.

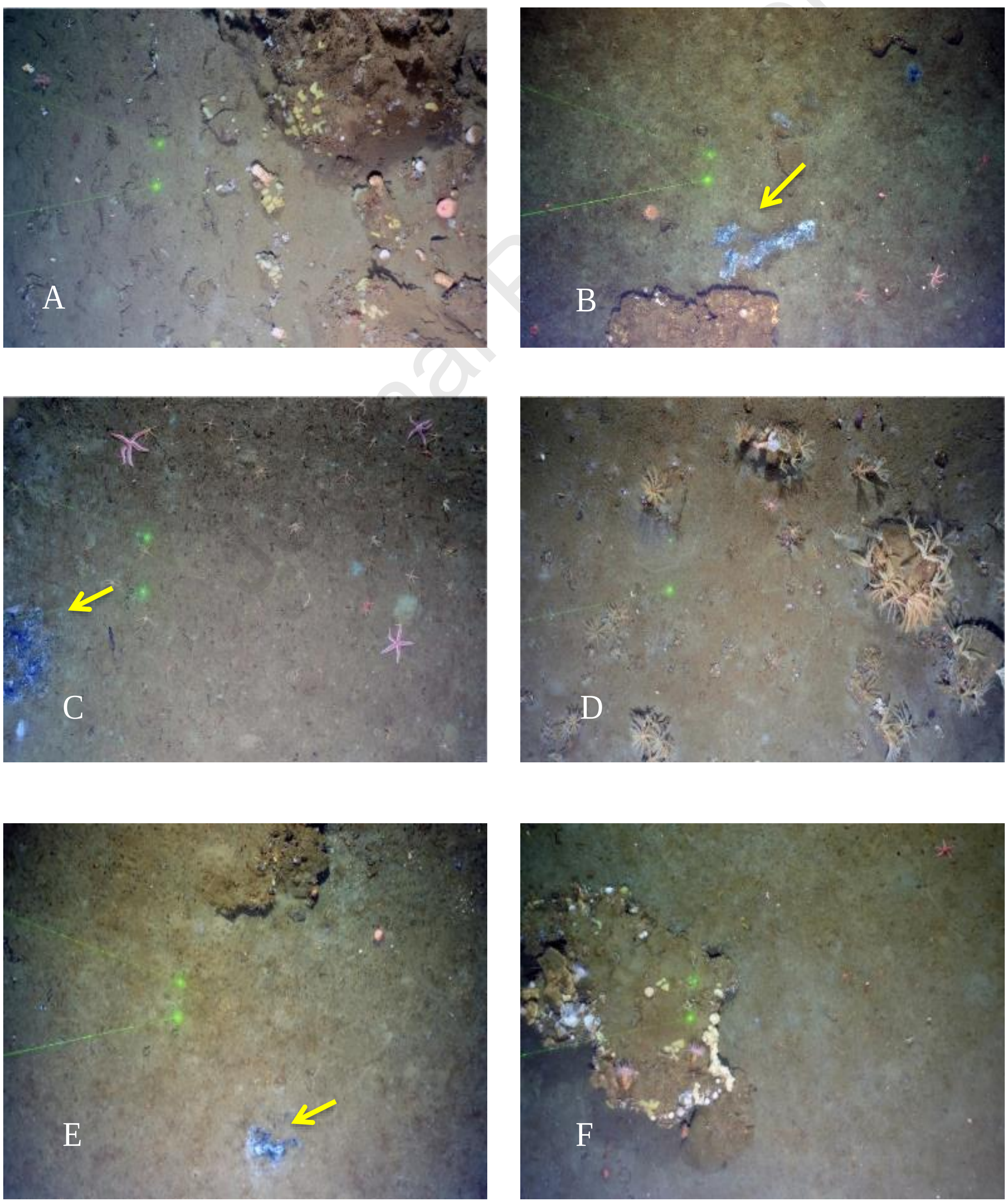

Figure 8A. The composition and distribution of biological community features outside the crater site (*TowCam* # HH942-23) within the Storbanken area. More than 16 megafaunal taxa were observed over 3 km of seafloor at the non-crater site. Fauna included multiple species of encrusting sponge, fish including schooling fish, soft corals, stalked crinoids, anemones, brittle stars, sea stars and psolid sea cucumbers**.**

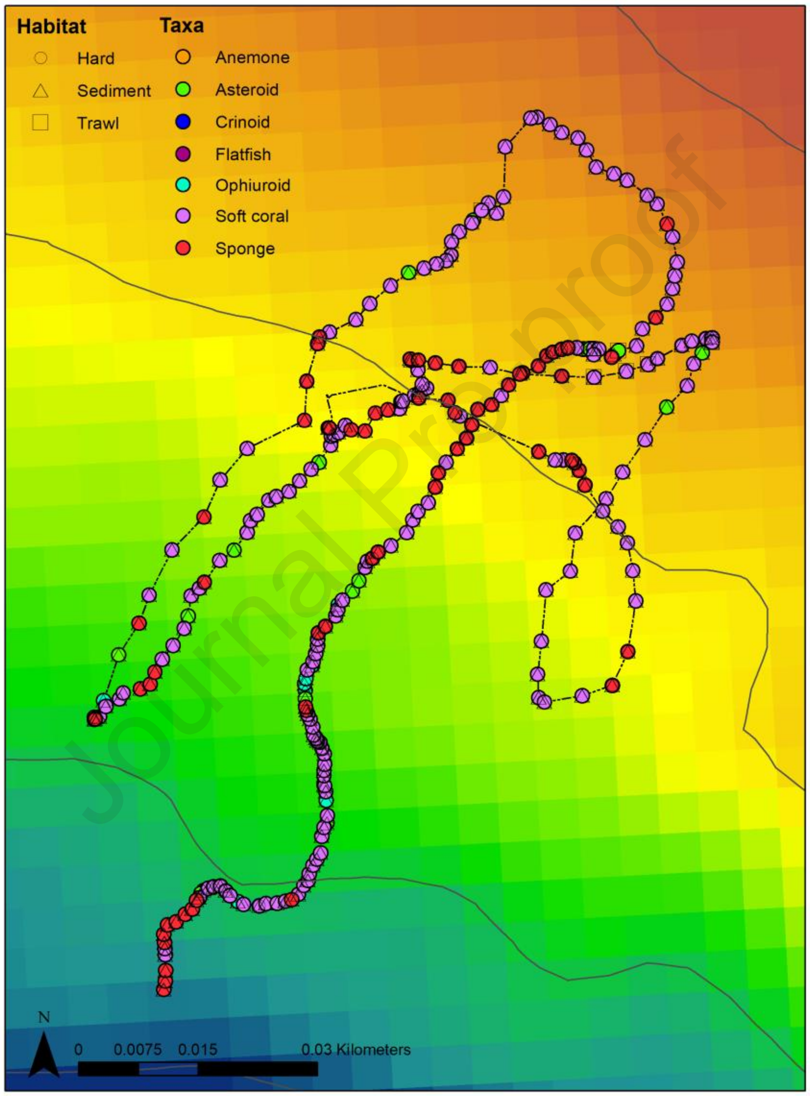

Figure 8B. The composition and distribution of biological community features inside the crater site (*TowCam* # HH942-25) within the Storbanken area.

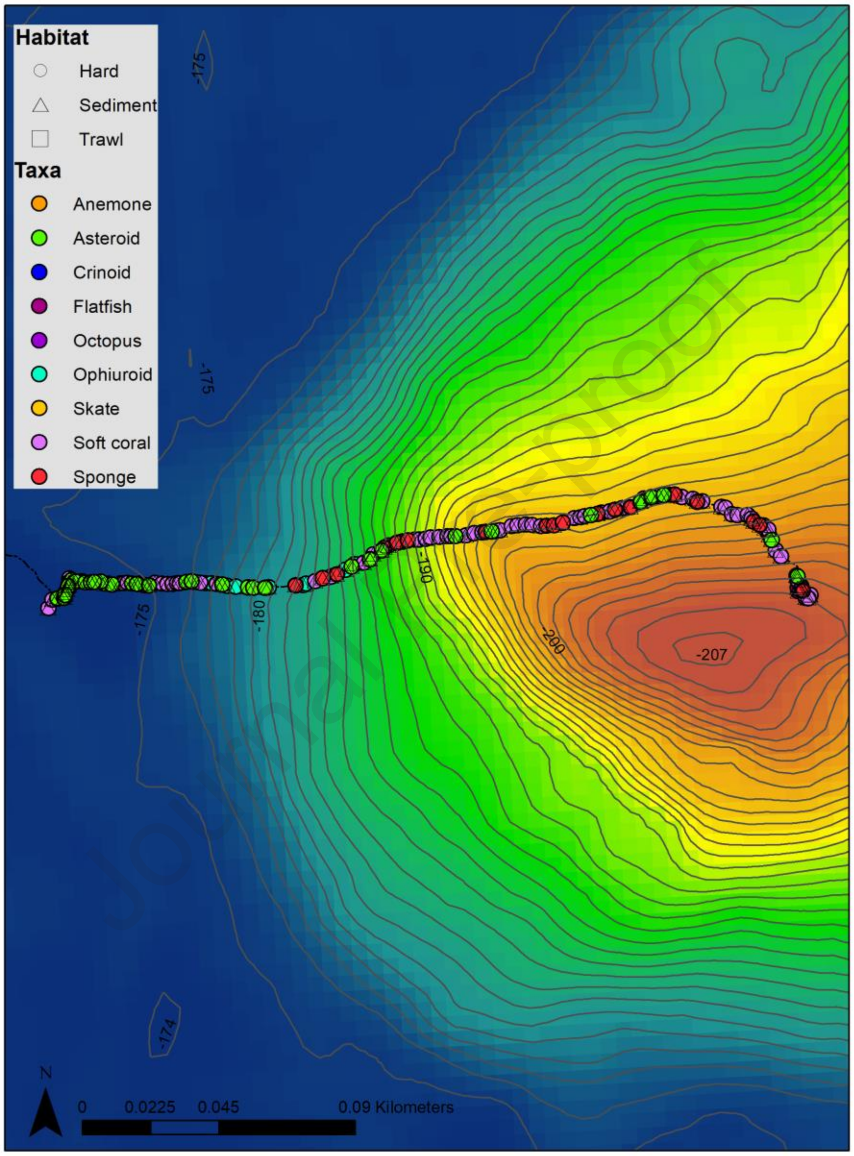

Table 1. Summary of 14 tows of the towed-camera system *TowCam* during cruise HH932 aboard the R/V *Helmer Hanssen* to investigate cold seeps in the Barents Sea in 2017. Green highlight indicates *TowCam* surveys at the crater site.

***TowCam* #**	**Site**	**Latitude**	**Longitude**	**Depth (m)**	**Dominant Seafloor Habitat**
HH932-TC13	1 km NE OBC	76 47.215	35 44.760	160	Soft Sediment
HH933-TC14	OBC-D1	76 46.737	35 43.457	220	Hard substrates
HH939-TC15	OBC-M1	76 46.840	35 11.188	155	Seep
HH940-TC16	OBC-M1	76 46.8657	35 13.895	155	Seep
HH942-TC17	OBC-M1	76 47.115	35 13.856	160	Rocky outcrop
HH947-TC18	OBC-D3	76 51.039	35 25.927	150	Seep and Carbonate crusts
HH948-TC19	OBC-D3	76 51.071	35 25.962	160	Seep and Carbonate crusts
HH950-TC20	OBC-D3	76 51.077	35 25.839	150	Seep
HH951-TC21	OBC-D3	76 51.095	35 25.905	160	Seep
HH957-TC22	OBC-D4	76 50.199	35 26.594	150	Soft Sediment
HH958-TC23	OBC-D3	76 51.104	35 25.893	150	Seep
HH962-TC24	OBC-C1	76 45.528	35 48.522	170	Soft Sediment
HH969-TC25	OBC-C1	76 45.903	35 49.492	200	Soft Sediment
HH970-TC26	OBC-C1	76 45.644	35 49.079	160	Rock

Table 2. Location of multicore (MC) and gravity core (GC) stations, the corresponding *TowCam* surveys and water depth at the sampling sites.

Station	*TowCam* Survey	Depth (m)	Latitude	Longitude	Relative position to Feature
MC-933	TC14	221	76 46.119	35 42.921	Within depression D1
MC-939	TC15	156	76 46.865	35 11.194	Proximal (<3 m) to microbial mat
MC-948	TC19	162	76 51.058	35 25.921	North of mapped MAREANO flare
MC-951	TC21	162	76 51.056	35 25.904	
MC-957	TC22	153	76 50.198	35 26.626	Close to microbial mat
MC-962	TC24	170	76 45.548	35 48.424	Close to mapped MAREANO flare
MC-969	TC25	202	76 45.920	35 48.974	Inside a crater
GC-935		191	76 46.842	35 30.915	Outside depression
GC-971		203	76 45.860	35 43.028	Inside depression (D1)
GC-972		203	76 45.859	35 43.033	Inside depression (D1)

Table 3.

Site	*TowCam* ID	Depth (m)	Microbial Mats	Bryozoa	Cnidaria (cf. *Drifa glomerata)*	Porifera	Arthropoda (shrimp; Caridea/ Dendrobranchia)	Arthropoda (Pycnogonid)	Arthropoda (Pagurid crabs)	Arthropoda (Brachyuran crabs)	Echinodermata (Holothuroidea cf. *Psolus*)	Echinodermata (Comatulid crinoid)	Echinodermata (Ophiuroidea)	Mollusca (Gastropod snails)	Mollusca (Octopoda)	Fish
1 km NE OBC	TC13	160	-	+	+ +	+ +	+	+ +	-	-	+	-	+ +	-	-	Small morphospecies
OBC-D1	TC14	220	-	+ +	+ +	+ +	+	+ +	-	+	+ +	-	+ +	-	+	cf. *Hippoglosoides platessoides*, large and small size class (schooling)
OBC-M1	TC15-TC17	155-160	+	+	+ +	+ +	-	-	-	-	+ +	+ +	+ +	-	-	cf. *Hippoglosoides platessoides*; small size class; cf. *Gadus mohua*
OBC-D3	TC18-TC21, TC23	150-160	+ +	+	+ +	+ +	-	-	+	-	+ +	+ +	+ +	+ +	-	cf. *Hippoglosoides platessoides*; small size class
OBC-D4	TC22	150	-	+	+ +	+ +	-	-	+	-	+ +	-	+ +	+ +	-	Small size class
OBC-C1	TC24-TC26	160-200	-	+	+ +	+ +	+	+ +	-	+	+ +	-	+ +	-	-	*cf. Hippoglosoides platessoides*; small size class; (schooling)

-	Not observed
+	Present, < than 10 indiv. per site
+ +	Present, > than 10 indiv. per site

Supplemental Material

Figure 1: Pore water concentration profiles of methane, dissolved iron and calcium in the multicores (left column) and gravity cores (right column). Note the different depth scales for the multicore and gravity plots.

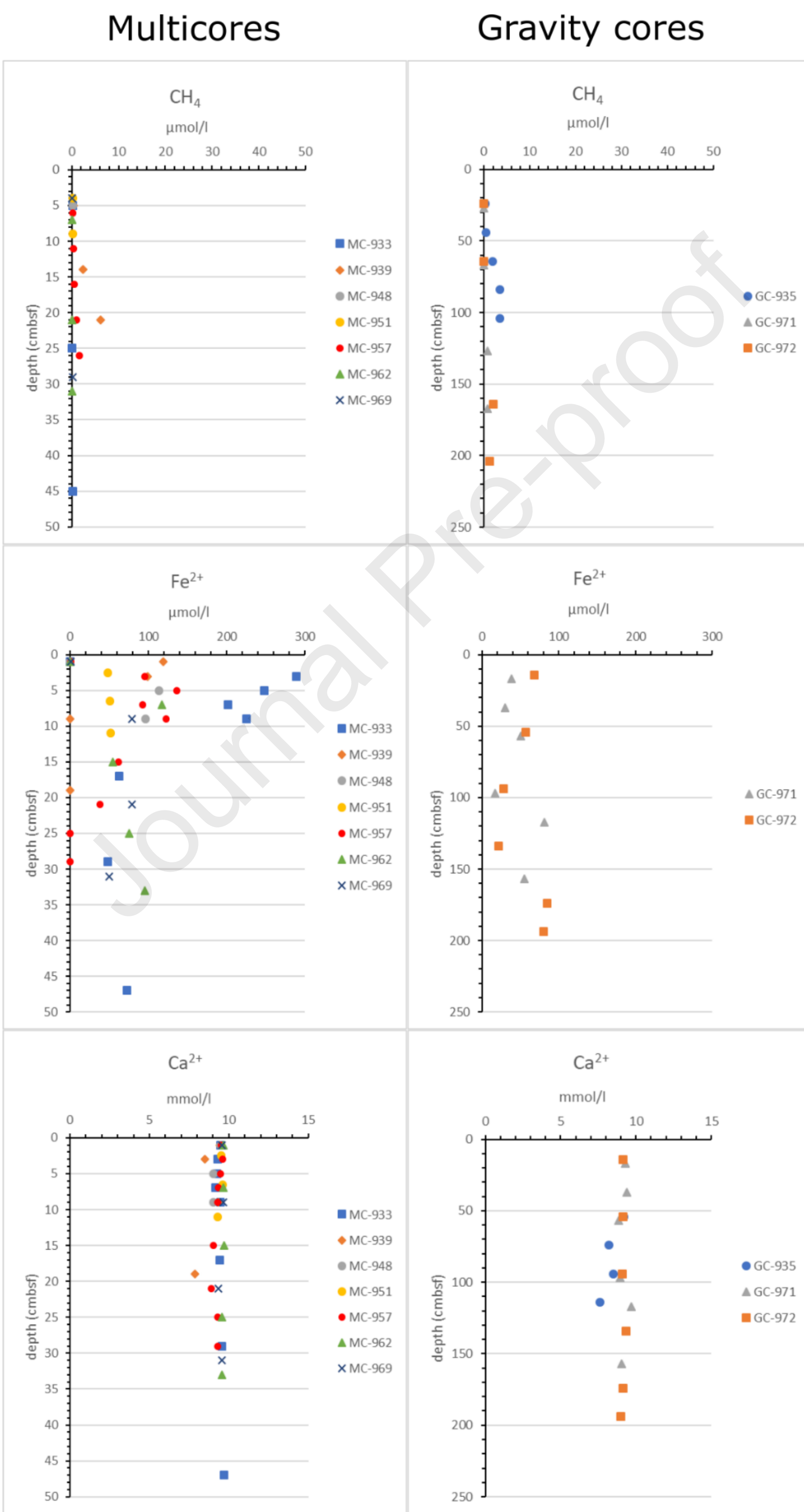

Figure 2: Pore water concentration profiles of strontium and boron in the multicores (left column) and gravity cores (right column). Note the different depth scales for the multicore and gravity plots.

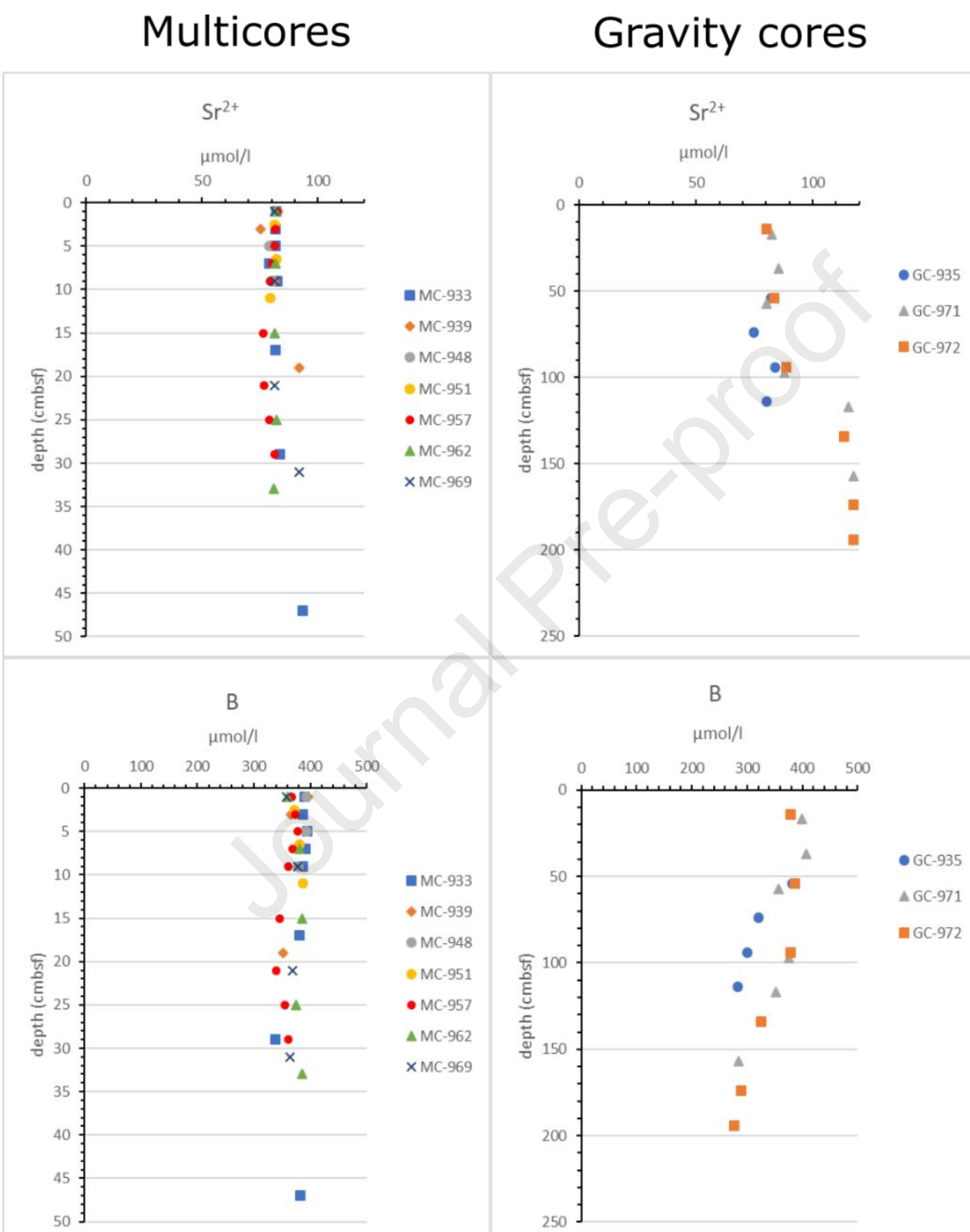

Figure 3: Pore water data of total alkalinity, dissolved inorganic carbon (DIC) and □[13]C-DIC for some of the multicores.

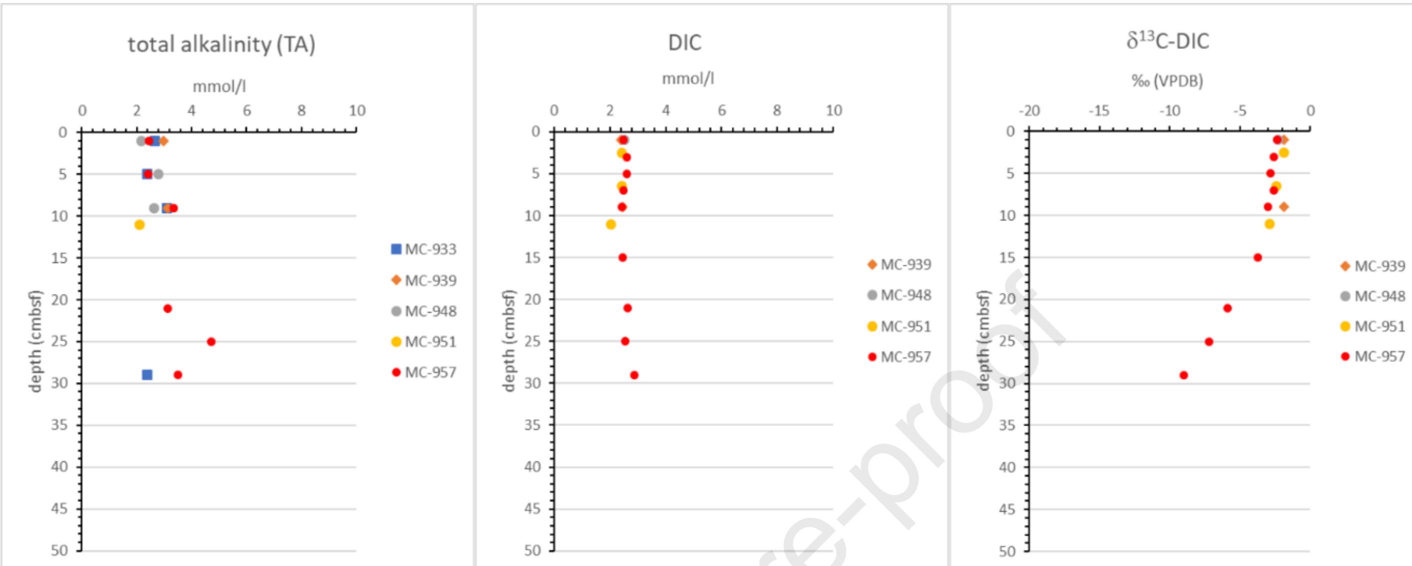

Table 1. Concentration measurements of pore water dissolved components and methane headspace of multicores and gravity cores from cruise CAGE 17-2.

	Depth	Fe^{2+}	Total alkalinity	$\square^{13}$C-DIC	DIC	Ca^{2+}	Sr^{2+}	B	Depth	CH_4
Core	*cm*	*µM*	*mmol/l*	*‰ (VPDB)*	*mmol/l*	*mmol/l*	*µmol/l*	*µmol/l*	*cm*	*µmol/l*
MC-933-5	1	0.0	2.7			9.5	82.1	390.4	5	0.2
	3	288.9				9.3	81.5	387.6	25	0.1
	5	248.2	2.4			9.3	81.7	394.1	45	0.2
	7	201.9				9.2	78.9	391.3		
	9	225.4	3.1			9.5	82.4	386.7		
	17	62.7				9.4	81.5	381.1		
	29	47.9	2.4			9.6	83.4	338.6		
	47	72.3				9.7	93.2	383.0		
GC-935	54		2.5			9.2	82.2	382.1	24	0.4
	74					8.2	74.9	320.1	44	0.5
	94					8.5	83.9	300.6	64	1.9
	114					7.6	80.2	282.1	84	3.5
									104	3.5
MC-939-5	1	119.0	3.0	-1.9	2.4	9.4	82.6	395.9	5	0.4
	3	99.3				8.5	75.2	366.3	14	2.5
	9	0.0	3.1	-1.9	2.5	9.4	81.1	378.4	21	6.1
	19	0.0				7.9	91.9	352.5		
MC-948-2	1	0.4	2.2	-2.3	2.5	9.5	82.4	393.2	5	0.2
	5	113.4	2.8			9.0	79.1	393.2		
	9	96.3	2.6			9.0	79.7	379.3		
MC-951-2	3	48.4		-1.9	2.4	9.5	81.3	371.9	4	0.3
	7	50.9		-2.4	2.4	9.6	82.2	380.2	9	0.1
	11	52.2	2.1	-2.9	2.0	9.3	79.3	386.7		
MC-957-5	1	0.9	2.5	-2.4	2.5	9.5	82.5	367.3	6	0.2
	3	95.4		-2.6	2.6	9.6	81.7	373.7	11	0.4
	5	136.1	2.4	-2.8	2.6	9.5	81.1	377.4	16	0.5
	7	92.9		-2.6	2.5	9.3	80.0	368.2	21	0.9
	9	122.4	3.4	-3.0	2.4	9.3	79.2	360.8	26	1.6
	15	61.6		-3.7	2.4	9.0	76.5	345.1		
	21	38.1	3.1	-5.9	2.6	8.9	76.6	340.4		

	25	0.0	4.7	-7.2	2.5	9.3	79.0	355.2		
	29	0.0	3.5	-9.0	2.9	9.3	81.1	360.8		
MC-962-5	1	0.0				9.7	81.6	359.9	7	0.1
	7	117.3				9.6	81.7	380.2	21	0.1
	15	54.4				9.7	81.4	384.8	31	0.1
	25	75.8				9.6	81.9	374.7		
	33	95.4				9.6	81.0	385.8		
MC-969-5	1	1.3				9.6	81.4	358.0	4	0.1
	9	78.8				9.6	81.3	377.4	29	0.3
	21	79.2				9.4	81.1	369.1		
	31	50.5				9.6	91.8	364.5		
GC-971	17	38.5				9.3	82.6	399.6	27	0.0
	37	30.4				9.4	85.3	407.0	67	0.0
	57	50.1				8.9	80.2	357.1	127	0.9
	97	17.1				8.9	88.0	374.7	167	0.8
	117	80.9				9.7	115.3	351.5		
	157	55.2				9.1	117.6	284.0		
GC-972	14	68.1				9.1	80.2	379.3	24	0.1
	54	57.4				9.1	83.5	385.8	64	0.0
	94	28.3				9.1	88.6	379.3	164	2.1
	134	21.4				9.4	113.4	325.6	204	1.4
	174	85.2				9.2	117.6	288.6		
	194	80.5				9.0	117.6	276.6		

Highlights

- Abundant methane flares observed along the Norwegian margin prior to 2015 and reduced number of flares detected in 2017, together with low methane concentrations measured in the sediment, suggest an inter-annual transient seep environment
- Metazoan community structure within the Storbanken Crater area in the Barents Sea revealed high diversity and differences between crater and non-crater sites
- We present the first evidence of methane release and flux with microbial mat distribution and associated folliculinid ciliates
- No chemosynthetic megafaunal species were observed among areas of seep expression in the areas surveyed
- We provide baseline information on the temporal release of arctic methane and benthic biological communities, initiating temporal studies to identify future changes and predict the impacts of climate change

Declaration of interests

☐ The authors declare that they have no known competing financial interests or personal relationships that could have appeared to influence the work reported in this paper.

☒ The authors declare the following financial interests/personal relationships which may be considered as potential competing interests:

Giuliana Panieri reports financial support was provided by UiT Centre for Arctic Gas Hydrate, Environment and Climate.